

UNIVERSITÉ DU QUÉBEC À MONTRÉAL

AJUSTEMENT DE L'ACCUMULATION DES PRÉCIPITATIONS SOLIDES EN FONCTION DU VENT ET DE
LA PHASE DES PRÉCIPITATIONS SUR LE BASSIN VERSANT DE BERSIMIS, QUÉBEC, CANADA

MÉMOIRE

PRÉSENTÉ

COMME EXIGENCE PARTIELLE

DE LA MAÎTRISE EN SCIENCES DE L'ATMOSPHÈRE

PAR

SARA-ANN PISCOPO

MARS 2023

UNIVERSITÉ DU QUÉBEC À MONTRÉAL
Service des bibliothèques

Avertissement

La diffusion de ce mémoire se fait dans le respect des droits de son auteur, qui a signé le formulaire *Autorisation de reproduire et de diffuser un travail de recherche de cycles supérieurs* (SDU-522 – Rév.04-2020). Cette autorisation stipule que «conformément à l'article 11 du Règlement no 8 des études de cycles supérieurs, [l'auteur] concède à l'Université du Québec à Montréal une licence non exclusive d'utilisation et de publication de la totalité ou d'une partie importante de [son] travail de recherche pour des fins pédagogiques et non commerciales. Plus précisément, [l'auteur] autorise l'Université du Québec à Montréal à reproduire, diffuser, prêter, distribuer ou vendre des copies de [son] travail de recherche à des fins non commerciales sur quelque support que ce soit, y compris l'Internet. Cette licence et cette autorisation n'entraînent pas une renonciation de [la] part [de l'auteur] à [ses] droits moraux ni à [ses] droits de propriété intellectuelle. Sauf entente contraire, [l'auteur] conserve la liberté de diffuser et de commercialiser ou non ce travail dont [il] possède un exemplaire.»

REMERCIEMENTS

Premièrement, je remercie ma directrice de recherche Julie Mireille Thériault pour sa présence, ses suggestions et son aide tout au long du projet de recherche. Je tiens à remercier Mitacs qui a couvert les dépenses liées à ce projet. Je remercie également mon collègue Nicolas Leroux pour son soutien, son partage de connaissance, son aide sur l'analyse des résultats, ainsi que l'aide avec l'écriture des programmes.

Enfin, je voudrais remercier Hydro-Québec, l'Institut de recherche en hydro-électricité et Dominique Tapsoba de m'avoir offert l'opportunité de travailler en leur collaboration, mais également de m'avoir fourni les données nécessaires à la réalisation de ce projet de recherche, sans compter le soutien offert par mes nombreux collègues tout au long de mon projet.

TABLE DES MATIÈRES

REMERCIEMENTS	ii
LISTE DES FIGURES.....	v
LISTE DES TABLEAUX	viii
LISTE DES ABRÉVIATIONS, DES SIGLES ET DES ACRONYMES.....	ix
RÉSUMÉ.....	x
CHAPITRE 1 INTRODUCTION	1
CHAPITRE 2 ADJUSTMENT OF SOLID PRECIPITATION ACCUMULATION AS A FUNCTION OF WIND AND PRECIPITATION PHASE OVER THE BERSIMIS WATERSHED, QUEBEC, CANADA	8
ABSTRACT	10
2.1 Introduction	11
2.2 Region of interest and datasets	14
2.2.1 Region of interest.....	14
2.2.2 Datasets used.....	14
2.3 Experimental design.....	16
2.3.1 Wind speed	16
2.3.2 Precipitation measurements	16
2.3.3 Phase partitioning method	17
2.3.4 Transfer functions	18
2.3.5 Data analysis	20
2.4 Results	21
2.4.1 Climatology	21
2.4.1.1 Precipitation.....	21
2.4.1.2 Wind speed	22
2.4.1.3 Air temperature	24
2.4.2 Phase partitioning.....	26
2.4.3 Corrected precipitation using various transfer functions.....	28
2.4.4 Phase partitioning use various methods and corrected solid precipitation amounts.....	30
2.5 Discussion.....	33
2.5.1 Phase partitioning methods.....	33
2.5.2 Range of accumulated snow	34
2.5.3 Evaluation of the solid precipitation.....	38
2.5.4 Implication on hydrology	42
2.6 Summary and Conclusions	42
2.6.1 Summary.....	42

2.6.2 Conclusions	43
CHAPITRE 3 CONCLUSION	46
APPENDIX A Station Lac à la Croix.....	50
APPENDIX B Méthodes de séparation pluie-neige.....	51
APPENDIX C Températures moyennes annuelles	52
APPENDIX D Résultats entiers des nuages de points de la Figure 2.18.	53
RÉFÉRENCES	54

LISTE DES FIGURES

Figure 1.1 : Schéma d’une jauge et d’un écran Tretyakov entourés du Double Fence Intercomparison Reference (DFIR) (Goodison et al., 1998).	3
Figure 2.1 Map of the Bersimis River Basin located in Quebec, Canada. (a) is a larger view on the basin showing the hypsometry; (b) indicates the location and name of each station used in this study... 14	14
Figure 2.2: Example of a Hydro-Quebec weather station. (a) is the view from the top and (b) shows precipitation and meteorological instruments with 2.5-m wind speed only. Photo from Hydro-Quebec Production. 2-m temperature sensor, 2.5-m wind speed and wind direction sensor, precipitation gauge covered by single-Alter shield and rain gauge.	15
Figure 2.3: Liquid fraction estimated by four different partitioning methods using temperature ranging from -10°C to 10°C. T0 represents the T = 0°C threshold, T2 represents the T = -2°C threshold, PQ represents the PQ linear threshold and Kienzle represents the Kienzle sigmoidal threshold.....	18
Figure 2.4: The collection efficiency (CE) of each transfer function as a function of wind speed, gauge height and 10-m wind speed combined. For equations dependent of air temperature, the solid lines modelling CE with respect to wind speed, represent T = -5°C and the dotted lines represent T = -10°C. For the equations dependent on snowfall intensity (SI), the solid lines modelling CE, with respect to wind speed, using SI = 1 mm h ⁻¹ and for the dotted lines, SI = 5 mm h ⁻¹ (Kochendorfer et al., 2017b). The acronyms are given in Table 2.2.	21
Figure 2.5: Yearly cumulated total precipitation [mm] for all 9 sites from October 2010 to April 2020. Croix and CDP are Lac à la Croix and Chute-des-Passes, respectively. Since Bonnard 1 and 2 have similar accumulated precipitations, only Bonnard 2 is visible.	22
Figure 2.6: Percentage of occurrence of the 10-m wind speed at each station during the winter months from 1 October 2010 to 30 April 2020. The location of the stations is given Figure 1. Wind speed bins used are 1 m s ⁻¹	23
Figure 2.7: Percentage of occurrence of the 2-m wind speed at each station during the winter months from 1 October 2010 to 30 April 2020. The location of the stations is given Figure 1. Wind speed bins used are 1 m s ⁻¹	23
Figure 2.8: Annual average number of hours for different temperature bins (bins of 4°C) for each station. The red bar highlights the temperature between -2°C and 2°C and the black vertical bar shows the mean temperature at each station over the whole period.....	24
Figure 2.9: Number of warm spells (temperature between -2°C and 2°C) per month for each station from 2010 to 2020. Croix represents Lac à la Croix and CDP represents Chute-des-Passes.	25
Figure 2.10: Annual accumulated number of warm spells per month over each hydrological year (October of the written year up to April of the next year) for each station (temperature between -2°C and 2°C).	26

- Figure 2.11: Percentage of snow for all station data for the three different partitioning methods (a) per hydrological year (e.g. 2010 is from October 2010 to April 2011) and (b) per month. The different partitioning methods are identified as T0 for the static threshold at $T = 0^{\circ}\text{C}$, T2 as the $T = -2^{\circ}\text{C}$ static threshold, PQ represents the linear transition method by Quick and Pipes (1977) and Kienzle represents the sigmoidal transition. 27
- Figure 2.12: Total accumulated liquid and solid precipitation (blue and orange, respectively) for a) partitioning method is 0°C or below, b) partitioning method solid when temperature is -2°C or below, c) Kienzle sigmoidal partitioning method (Kienzle, 2008) and d) Quick and Pipes (1977) partitioning method for each station over 10 years for warm spells (temperature between -2°C and 2°C). Croix represents Lac à la Croix and CDP represents Chute-des-Passes. Note that due to the filtering method and requirements needed to apply the transfer functions, the number of hourly samples differ for each site (Table 2.1). 28
- Figure 2.13: (a) Measured and adjusted accumulated solid precipitation from 1 October 2010 to 30 April 2020, at each station. Solid precipitation is assumed to be at 0°C (T0) and 16 transfer functions were used. (b) Mean annual corrections (mm y^{-1}) from 1 October 2010 to 30 April 2020 per station for the 16 transfer functions. Acronyms shown in the legend are defined in Table 2.2. Croix represents Lac à la Croix and CDP represents Chute-des-Passes. 29
- Figure 2.14: Total amount of precipitation (mm) from 2010 to 2020 for the months of October to April for each station for the different phase partitioning methods. a) partitioning method is 0°C or below, b) partitioning method solid when temperature is -2°C or below, c) Kienzle sigmoidal partitioning method (Kienzle, 2008) and d) Quick and Pipes (1977) partitioning method. 31
- Figure 2.15: The solid cumulated precipitation percentage with the 2-m wind speed (U) effect using the coefficients and equations over the period of 2010 to 2020 for the months of October to April using the $T=-2^{\circ}\text{C}$ partitioning method for available stations. 32
- Figure 2.16: Additional corrected solid precipitation amounts relative to measurements (%) with the 10-m wind speed (U) equations for the period of 2010 to 2020 for the months of October to April using the $T=-2^{\circ}\text{C}$ partitioning method. 33
- Figure 2.17: The percentage of additional cumulated snow from 2010 to 2020 for the months of October to April for each station for the different phase partitioning methods. a) partitioning method is 0°C or below, b) partitioning method solid when temperature is -2°C or below, c) Kienzle sigmoidal partitioning method (Kienzle, 2008) and d) Quick and Pipes (1977) partitioning method. 35
- Figure 2.18: Scatter plot of the corrected and uncorrected hourly precipitation [mm] for each partitioning method over the range of temperature between -4°C and $+8^{\circ}\text{C}$. Each line represents a different equation, starting with NOR10, followed by U2 and lastly USA2_SI, described in Table 2. The columns and colours represent the partitioning methods, where blue is the T0 method, orange is T2, red Kienzle and PQ in green. Mbias represents the mean bias between corrected and uncorrected hourly precipitation (Equation 2.5). Data from Chute-des-Passes is illustrated here since it has the highest total precipitation. 37
- Figure 2.19: Total cumulated measured and corrected solid precipitation from 2010 to 2020 for the months of October to April for each station compared to ERA5 reanalysis data (pink). a) partitioning method

is 0°C, b) partitioning method solid when temperature is -2°C or below, c) Kienzle sigmoidal partitioning method and d) Quick and Pipes (1977) partitioning method..... 39

Figure 2.20: Annual cumulated mean solid precipitation for measured and corrected solid precipitation from 2010 to 2020 for the months of October to April for each station compared to ERA5 reanalysis data (pink). a) partitioning method is 0°C, b) partitioning method solid when temperature is -2°C or below, c) Kienzle sigmoidal partitioning method and d) Quick and Pipes (1977) partitioning method. 40

Figure 2.21: Mean annual bias per station of ERA5's solid precipitation estimation compared to the corrections and uncorrected solid precipitation data for the six transfer functions illustrated by partitioning method for a) temperature threshold is 0°C, b) temperature threshold is -2°C or below, c) Kienzle sigmoidal transition and d) Quick and Pipes (1977) linear transition. 41

LISTE DES TABLEAUX

Table 2.1: The station used in this study. The longitude, latitude and site elevations are given. Hourly samples are the number of samples after applying the quality control procedure described in section 2.3.2.	15
Table 2.2: Transfer functions used to correct for precipitation wind undercatch (Kochendorfer et al., 2017a, 2017b and Colli et al., 2020). The wind speed is in m s^{-1} and the air temperature is $^{\circ}\text{C}$	19
Table 2.3: Annual mean bias percentage for Chute-des-Passes station using the T2 threshold method for winter years of 2010 to 2020. Equations are classified in various groups from A to F. The classification was grouped by similarity in bias values.	30

LISTE DES ABRÉVIATIONS, DES SIGLES ET DES ACRONYMES

C3S Copernicus Climate Change Service

CDP Chute-des-Passes

CE Collection Efficiency

Croix Lac à la Croix

DFIR Double Fence Intercomparison Reference

EC Environment and climate change Canada

ECMWF European Center for Medium-Range Weather Forecasts

ERA5 ECMWF Reanalysis version 5

GMON Gamma MONitor

HQ Hydro-Quebec

IMERG Integrated Multi Satellite Retrievals for Global Precipitation Measurement

MERN Quebec Ministry of Energy and Natural Resources

OMM Organisation Météorologique Mondiale

PQ Quick and Pipes

RT Rio Tinto

SDFIR Small DFIR

SWE Snow Water Equivalent

WMO SPICE World Meteorological Organization Solid Precipitation Intercomparison Experiment

RÉSUMÉ

La quantité d'eau disponible au printemps est critique pour la production hydro-électrique. Hydro-Québec, un producteur d'hydro-électricité, a besoin d'estimations plus fiables du stock d'eau maximal lors de la fonte de la neige afin d'améliorer ses prévisions hydrologiques. De meilleures estimations peuvent être obtenues à l'aide de mesures de précipitations solides plus précises. Mesurer avec précision les précipitations solides durant l'hiver demeure complexe, car il est connu depuis des décennies que les quantités de précipitations solides mesurées diminuent avec l'augmentation de la vitesse du vent. Cette forte sous-captation de précipitations peut conduire à une sous-estimation significative des quantités de neige tombées pendant les saisons hivernales, ce qui a un impact sur la quantité d'eau disponible au printemps. Des fonctions de transfert sont utilisées pour ajuster la sous-captation des précipitations solides déviées par le vent. Ce mémoire présente un éventail de précipitations solides corrigées sur le bassin de la rivière Bersimis, un bassin versant situé au Québec où Hydro-Québec produit de l'hydro-électricité. À cet effet, des fonctions de transfert développées lors de l'expérience WMO-SPICE ont été appliquées pour ajuster les quantités horaires de précipitations utilisées par Hydro-Québec à neuf stations à partir de 2010 jusqu'en 2020. Étant donné que seules les précipitations solides doivent être ajustées, différentes méthodes de séparation des phases ont été utilisées, laissant un total de 24 combinaisons d'ajustement des précipitations solides. Dans l'ensemble, la méthode de partition utilisant une transition sigmoïdale a obtenu la quantité de précipitations solides la plus élevée, alors que la méthode du seuil de température fixe à -2°C a calculé la quantité la plus faible. Quant aux fonctions de transfert, les équations norvégiennes de Kochendorfer et al. (2017a ; 2017b) ont donné les plus grandes corrections de précipitations solides. Les résultats dépendent fortement de la vitesse du vent, ainsi que des épisodes de températures supérieures à 0°C pendant la saison froide. L'éventail de corrections des précipitations solides corrigées durant un hiver varie de 15 à 100 mm supplémentaires selon l'équation et la méthode de séparation des phases choisie. La réanalyse v5 (ERA5) du Centre européen pour les prévisions météorologiques à moyen terme (ECMWF) a montré une grande variabilité lors d'une comparaison avec l'éventail de résultats obtenus. Dans l'ensemble, cette étude a démontré le besoin d'ajuster les mesures de précipitations solides sur le bassin de Bersimis. Ceci permettrait notamment d'émettre un éventail de prévisions hydrologiques à l'approche des crues printanières dans le but d'améliorer la gestion de l'eau pour la production d'énergie hydro-électrique.

CHAPITRE 1 INTRODUCTION

Les précipitations sont la source primaire de plusieurs ressources en eaux exploitées dans de nombreuses activités humaines (agronomie, production hydro-électrique, etc.). Elles existent sous forme liquide, solide ou un mélange de solide et liquide (phase mixte). Leurs caractérisations sont essentielles pour la gestion de ces différentes ressources qu'elles engendrent d'une part, mais aussi celle de plusieurs aléas qu'elles occasionnent d'autre part, par exemple, les inondations (Cloke et Pappenberger, 2009; Devia et al., 2015; Larson et Peck, 1974). Les inondations peuvent avoir plusieurs impacts sur l'économie, sur la santé publique au Québec, mais aussi dans de nombreux pays du monde (WMO, 2014). Un usage optimal et sécuritaire de cette ressource essentielle soulève le besoin de quantifier les ressources en eau de surface et son évolution au cours du temps, ce qui est intimement lié aux précipitations à travers le cycle hydrologique. L'importance d'avoir de bonnes mesures de précipitations est également justifiable pour la validation des modèles atmosphériques et hydrologiques, ainsi que pour étudier la variabilité climatique (Yang et al., 2005). De ce fait, une bonne méthode de mesure des quantités d'eau et une bonne compréhension des phénomènes associés aux précipitations permettent une gestion optimale de l'eau pour la société, non seulement en termes de ressource, mais également en termes de limitation des conséquences reliées aux catastrophes naturelles.

La mesure de la précipitation est un exercice difficile, notamment aux latitudes moyennes où l'occurrence de précipitation en phase mixte s'ajoute à la difficulté de quantifier les précipitations solides puisque des changements de phases sont parfois présents durant l'hiver (Goodison et al., 1998 ; Rasmussen et al., 2001). En effet, les biais reliés aux mesures de précipitations solides peuvent atteindre plus de 50 % lors de l'utilisation de différentes technologies (Rasmussen et al., 2012 ; Yang et al., 1999). À ce jour, il existe une multitude de techniques et de types d'instruments permettant de mesurer les précipitations. Parmi ces méthodes, on trouve des jauges de type manuelle, des jauges automatiques, des disdromètres, ainsi que des plaques chauffantes (Goodison et al., 1998 ; Rasmussen et al., 2002 ; Rasmussen et al., 2012). Tout instrument comporte ses erreurs systématiques, de mesure et de précision. D'autres facteurs peuvent également altérer l'exactitude des mesures.

Plusieurs facteurs peuvent affecter la mesure des précipitations solides. Les erreurs associées aux pertes dues à l'évaporation et à la sublimation des hydrométéores, contenu dans la jauge, en est un exemple. Cette source d'erreur est présente dans tous les types de jauges où l'orifice est à aire ouverte. Leeper et

Kochendorfer (2015) ont démontré que les jauges massiques dépourvues de liquide anti-évaporant peuvent perdre en moyenne jusqu'à 0.12 mm h^{-1} dû à l'évaporation. L'amplitude de ce biais varie en fonction du type de jauge, la présence ou non de liquide anti-évaporation et est beaucoup plus important en été qu'en hiver (Leeper et Kochendorfer, 2015 ; Goodison et al., 1998). Pour diminuer les pertes associées à ce type d'erreur, il est possible de mettre de l'huile à l'intérieur de la jauge ce qui prévient l'évaporation/sublimation des précipitations (Rasmussen et al., 2012). Une autre source d'erreur que l'on peut rencontrer lors de la mesure des précipitations solides est l'accumulation de la neige en bordure de l'instrument de mesure. Ce problème est présent pour les jauges ayant une ouverture horizontale comme les jauges à peser telles que le Geonor, Inc. ou le Pluvio OTT (Messtechnik, Germany). Lorsque l'accumulation de neige en bordure de l'instrument est présente, l'embouchure de l'instrument peut être complètement ou partiellement obstruée, ou encore, que l'accumulation de neige en bordure tombe à l'intérieur ou l'extérieur de l'instrument de mesure. Afin de diminuer les effets de ce type d'erreur, certains instruments sont équipés d'un anneau chauffant, ce qui évite les accumulations de neige à l'entrée des jauges (Rasmussen et al., 2001). Aussi, l'effet du vent sur la neige au sol peut créer un courant d'air ascendant entraînant la neige au-dessus du niveau du sol et l'amener à l'intérieur de la jauge, ajoutant une nouvelle erreur de mesures de la neige.

L'effet du vent qui fait dévier les flocons de l'orifice de l'instrument demeure la source d'erreur principale pour toutes les jauges de précipitations. Sevruk (1989) a démontré que la présence d'une jauge déforme le flux d'air, ce qui cause une déviation du flocon à l'extérieur de la jauge. Ce type d'erreur systématique est connue sous le nom de sous-captation due au vent (Goodison et al., 1998 ; Rasmussen et al., 2012). Plusieurs scientifiques ont tenté de quantifier cette erreur afin de diminuer son effet en testant l'ajout d'écrans ou de paravents autour de l'instrument (ex : Yang et al., 1998 ; Smith, 2009 ; Rasmussen et al., 2012 ; Goodison et al., 1998). Comme pour les jauges, il existe plusieurs types d'écrans : simple ou double-Alter (Alter, 1937), Tretyakov, buisson (*bush*), Nipher (Nipher, 1878), Double Fence Intercomparison Reference (DFIR) (Golubev, 1989 ; Yang et al., 1993) et le Small-DFIR (SDFIR, Nitu et al., 2019).

Diverses études ont été réalisées afin de quantifier les erreurs associées aux différents paravents que l'on peut retrouver (Goodison, 1978 ; Sevruk et al., 1991 ; 2009 ; Goodison et al., 1998 ; Smith, 2009 ; Wolff et al., 2015 ; Kochendorfer et al., 2017a ; Buisán et al., 2017). Entre autres, l'Organisation Météorologique Mondiale (OMM) a réalisé une campagne de terrain WMO SPICE (World Meteorological Organisation Solid Precipitation Intercomparison Experiment) dans plusieurs pays pour étudier et quantifier la mesure les

précipitations solides. Cela leur a permis de tester les différents instruments de mesure avec et sans écrans. Plusieurs sites ont été utilisés lors de cette expérience afin de prendre en compte les effets des divers climats hivernaux sur les précipitations solides, d'améliorer les connaissances sur la mesure de l'équivalence en eau de la neige et permettre le partage des résultats obtenus. Il a été démontré qu'une jauge entourée d'un buisson, sans feuille, maintenue à la même hauteur que l'instrument, obtient une efficacité de collecte de précipitations qui correspond aux quantités réelles de précipitations, et ce, pour différentes vitesses de vent (Goodison et al., 1998). Un second instrument de référence, le DFIR, fut également désigné pour contrer les multiples problèmes reliés au climat nécessaire pour faire pousser un buisson et d'éviter l'entretien relié à la hauteur de celui-ci (DFIR ; Groisman et al., 1991 ; Yang, 2014). Le DFIR est une jauge manuelle Tretyakov entourée de deux écrans de forme octogonale verticale (Figure 1.1 ; Goodison et al., 1998). Depuis, il est maintenant commun que les DFIR soient équipés de jauges massiques accompagnés d'un écran Alter (Kochendorfer et al., 2017a ; 2017b). Les boucliers permettent de diminuer la vitesse du vent à l'orifice des jauges, tandis que les types de jauges massiques tels que les Geonor ou encore les OTT Pluvio obtiennent généralement des résultats similaires (Kochendorfer et al., 2017b). De plus, on remarque que l'accumulation mesurée par les différentes combinaisons jauge-écran se disperse davantage à mesure que la vitesse du vent augmente (Thériault et al., 2012).

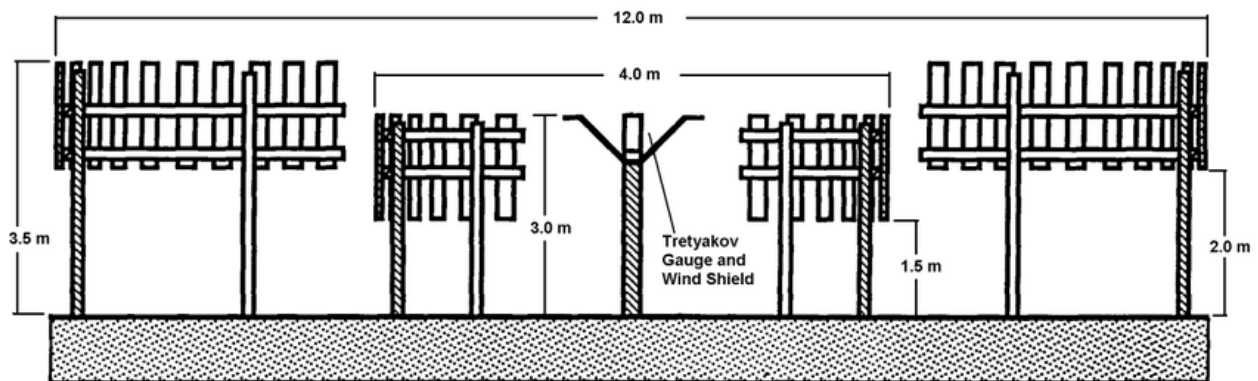


Figure 1.1 : Schéma d'une jauge et d'un écran Tretyakov entourés du Double Fence Intercomparison Reference (DFIR) (Goodison et al., 1998).

Afin de quantifier le degré de sous capture des différents instruments, un rapport a été établi afin de créer des équations de transfert. Par définition, l'efficacité de collecte (*Collection Efficiency*) (CE) représente le rapport entre la quantité de précipitation recueillie par une jauge quelconque sur la quantité de précipitation captée par un des deux instruments de référence. Grâce à ce rapport, il est possible d'évaluer l'écart de mesure qu'une certaine jauge aurait par rapport à la réalité. Lorsque la vitesse du vent

augmente, l'efficacité de collecte des flocons diminue. Par conséquent, la vitesse du vent est inversement proportionnelle à l'efficacité de collecte de la jauge. Pour des vitesses de vent de 5 m s^{-1} , les erreurs de mesure pour une jauge de type Geonor avec écran Alter simple peuvent atteindre jusqu'à 64 % sans facteur de correction (Rasmussen et al., 2012). Par exemple, on peut voir que l'efficacité de collecte relative à l'instrument de référence démontre que le CE pour un bouclier simple Alter est moins élevé que pour un bouclier double Alter.

Goodison et Yang (1996) ont mentionné que le biais dû à la sous captation du vent dépend de plusieurs facteurs soit : la vitesse du vent, la température, le type de précipitation et la configuration de la jauge. Pour parvenir à minimiser les erreurs de mesure des précipitations solides, des équations de transfert à partir de CE sont utilisées. Plusieurs fonctions de transfert ont été développées pour différents climats servant à réduire le biais relié à la sous-captation due au vent. L'avantage de ces équations est d'obtenir les mesures des précipitations corrigées, tout en gardant l'instrumentation facile d'accès et de plus petite taille (environ 1-2 m de diamètre) qu'un DFIR (environ 12 m).

Plusieurs campagnes de mesures ont été mises en place pour tenter de mieux quantifier l'effet du vent. Goodison (1978) a lancé l'expérience de Cold Creek Study sur quatre sites à travers le Canada afin de tester les effets de trois différents instruments, avec et sans écran, en conditions hivernales. Cette expérience a démontré que l'efficacité de collecte moyenne des précipitations peut s'exprimer comme une fonction exponentielle décroissante lorsque la vitesse du vent croît. Toutefois, cette conclusion s'applique pour deux des trois jauges testées, donc applicable pour la jauge Fisher et Porter et la jauge Belfort, mais exclu la jauge canadienne Nipher. L'expérience a également démontré que l'amplitude de l'efficacité de collecte des jauges dépend de la vitesse du vent ainsi que de la température, puisque l'effet du vent influence la forme des flocons qui dépend de la température (Goodison, 1978). Ensuite, deux expériences de WMO-SPIICE, la première a eu lieu en 1990, et la seconde en 2012, ont permis de regrouper une multitude de pays afin de tester dans différentes situations climatiques et de tester les effets de l'utilisation de plusieurs instruments de mesure pour les précipitations solides. La première phase de l'expérience a permis de déterminer l'instrument de référence (Goodison et al., 1998; Yang et al., 1995; Yang et al., 1998) et de créer des fonctions de transfert pour des jauges majoritairement manuelles. Toutefois, le besoin d'améliorer la mesure des précipitations solides a motivé le lancement d'une seconde phase de WMO-SPIICE en 2012. Celle-ci a notamment permis la création d'une base de données diversifiée en termes de

climat afin de comprendre le fonctionnement de jauges automatiques, des différents écrans disponibles et de développer des fonctions de transfert pour les instruments en question.

Ces expériences ont permis de développer diverses fonctions de correction telles que Wolff et al. (2015), Kochendorfer et al. (2017a ; 2017b ; 2018), Colli et al. (2020). Ces fonctions de transfert permettent d'obtenir de meilleurs résultats que les précédentes (Førland et al., 1996), car elles s'appliquent à des vitesses de vent < 9 m/s. Ces nouvelles fonctions de transfert s'appliquent aussi directement aux stations météorologiques automatiques, cependant, on remarque une grande dispersion dans les données pour une même vitesse de vent (Rasmussen et al., 2012). Cette dispersion s'explique principalement par le type de flocon de neige (Thériault et al., 2012); la neige mouillée ou givrée conduira à une meilleure efficacité de collecte que de la neige sèche. Cette différence s'explique principalement par leur vitesse de chute (Leroux et al., 2021).

Il est bien important de comprendre la microphysique des précipitations, car elle permet de déterminer le type de phase et les types de cristaux de neige qui peuvent être présents, améliorant ainsi la correction des précipitations hivernales (Rasmussen et al., 2012 ; Thériault et al., 2012). Ceux-ci peuvent se distinguer par leur type, leur densité, leur forme, leur fraction solide/fondue, leur degré d'agrégation, leur taille ainsi que leur vitesse de chute (Stewart et al., 2015). Parallèlement, la vitesse de chute est directement proportionnelle au type de précipitation (Thériault et al., 2012), qui à son tour impacte le degré de déviation des précipitations solides à l'entrée de la jauge.

Lors de températures proches de 0°C , il est possible d'observer des précipitations sous forme liquide, solide ou en phase mixte. Les fonctions de transfert utilisées sont uniquement dédiées aux précipitations solides, il est donc primordial de déterminer la phase de la précipitation pour éviter de prendre en considération les précipitations liquides. Le type de phase fait varier le type de précipitation, non seulement en surface, mais également en altitude puisque la température et l'humidité varient dans la colonne atmosphérique. Lorsque des précipitations solides traversent une couche plus chaude (température du thermomètre mouillée supérieure à 0°C), celles-ci peuvent changer de phase. De ce fait, ceci peut former des précipitations partiellement fondues, totalement fondues ou encore de la neige mouillée, en fonction de l'épaisseur de la couche chaude. À l'inverse, si des précipitations liquides traversent une couche de température négative, elles gèleront si la température est très froide ou si un noyau glaçogène est présent dans la particule. Ce processus mène à de la pluie verglaçante ou se solidifier

complètement pour former du grésil (Stewart et al., 2015 ; Glickman, 2000 ; Thériault et al., 2006 ; Libbrecht, 2005 ; etc.).

Il existe plusieurs méthodes pour estimer la fraction liquide des précipitations. La fraction liquide est le ratio de précipitation liquide sur la précipitation totale (Pipes et Quick, 1977). Cette variable est essentielle pour déterminer la quantité de précipitation solide nécessaire à l'application des équations de transfert pour la sous-captation par le vent (Kochendorfer et al., 2017a ; Colli et al, 2020 ; Wolff et al., 2015), mais est également un intrant important lors de la modélisation hydrologique et météorologique (Irannezhad et al., 2015). La fraction liquide dépend de la température à 2 m, les épaisseurs des couches atmosphériques, de l'humidité relative, puis, en fonction du climat ou de la région convoitée, d'un ou de plusieurs seuils de température où l'on distingue les précipitations solides des précipitations liquides (Gray and Prowse, 1993). Il est commun d'utiliser un seul seuil de température pour différencier la pluie de la neige (Kochendorfer 2017a). Par cette méthode, la fraction liquide ne peut être égale qu'à 1 ou 0, ce qui signifie que les précipitations sont quantifiées comme entièrement liquides ou solides. Il existe d'autres méthodes pour estimer la fraction liquide et solide qui permettent d'obtenir des précipitations mixtes, telles que l'utilisation d'un double seuil définissant les limites des précipitations liquides et solides ainsi qu'une transition linéaire entre les deux phases permettant la quantification de précipitations mixtes (Pipes et Quick, 1977). Similairement, il existe une méthode de calcul de la fraction liquide à double seuil offrant une transition sigmoïdale par Kienzle (2008). Cette méthode permet notamment de corriger les critères en fonction des saisons ainsi que de les calibrer en fonction du site directement. Finalement, Harder et Pomeroy (2013) proposent l'utilisation de la température du thermomètre mouillé afin de prendre en compte l'humidité relative contenue dans l'air pour estimer la fraction liquide et solide.

Il est nécessaire d'effectuer un suivi continu des précipitations durant l'hiver, ce qui s'avère une tâche nécessaire pour assurer une gestion optimale des systèmes hydriques, spécialement lors de la fonte de la neige pour des fins de gestion de l'eau (Larson et Peck, 1974). Il est important de diminuer les erreurs de mesure reliées aux précipitations hivernales pour mieux quantifier et prévoir les quantités d'eau qui se retrouveront dans les bassins versants, autant pour les besoins opérationnels dans le but d'avoir une meilleure gestion des ressources que pour les prévisions d'inondations printanières. En effet, l'équivalence en eau des précipitations solides est un intrant existentiel dans les modèles hydrologiques chez Hydro-Québec (Brown et al., 2018). L'objectif principal de ce mémoire est de caractériser l'accumulation de précipitation annuelle corrigée sur le bassin versant de Bersimis, Québec, Canada. Jusqu'à neuf stations

météorologiques sur les bassins de Bersimis 1 et 2 sont utilisées. Plusieurs méthodes de partitions de la phase sont utilisées pour déterminer la quantité de précipitation horaire. Ensuite, les précipitations solides sont corrigées à l'aide de plusieurs méthodes de correction des précipitations solides obtenues lors de la WMO-SPICE (Kochendorfer et al., 2017a ; 2017b ; 2018 ; Wolff et al. 2015 ; Goodison et al., 1998).

Cette étude est présentée sous forme d'un article scientifique qui sera soumis au journal Atmosphere-Ocean. L'article est organisé de la façon suivante : la première partie comprendra une description des différentes méthodes de calcul de la fraction liquide ainsi que des multiples équations de transfert pour la sous-captation due au vent. Par la suite, une étude climatologique des stations météorologiques sur 10 ans est réalisée afin d'anticiper et de comprendre les diverses réponses des équations proposées. Finalement, une analyse des résultats est détaillée et comparée aux Réanalyses du Centre Européen des prévision Météorologiques à Moyen Terme (ECMWF) version 5 (ERA5).

CHAPITRE 2 ADJUSTMENT OF SOLID PRECIPITATION ACCUMULATION AS A FUNCTION OF WIND AND PRECIPITATION PHASE OVER THE BERSIMIS WATERSHED, QUEBEC, CANADA

Ce chapitre est présenté sous forme d'un article scientifique rédigé en anglais qui sera soumis à *Atmosphere-Ocean*. L'article a été coécrit par Sara-Ann Piscopo, Julie M. Thériault, Nicolas Leroux et Dominique Tapsoba. Nicolas Leroux a aussi contribué à la préparation et l'analyse des données. Julie M. Thériault et Dominique Tapsoba ont supervisé le travail de recherche.

**Adjustment of Solid Precipitation Accumulation as a Function of Wind and Precipitation Phase over the
Bersimis River Basin, Quebec, Canada**

Sara-Ann Piscopo¹, Julie M. Thériault¹, Nicolas R. Leroux¹ and Dominique Tapsoba²

¹*Centre ESCER, Department of Earth and Atmospheric Sciences, Université du Québec à Montréal*

²*Hydro Québec, Institut de Recherche d'Hydro-Québec, Varennes, Québec, Canada*

Mars 2023

ABSTRACT

The amount of water available during the melt season is critical for hydropower production. Hydro-Québec, a hydropower producer, needs for better estimations of the maximal water stock during the snowmelt to improve hydrological forecasts, which can be obtained with precise solid precipitation measurements. Accurately measuring solid precipitation during the cold season is challenging because it is known for decades that the measured solid precipitation quality decreases with increasing wind speed. This solid precipitation undercatch can lead to a significant underestimation of snowfall amounts during the winter season, which impacts the amount of water available during spring. Transfer functions are used to adjust for solid precipitation undercatch because of the wind speed. This paper presents a range of corrected annual solid precipitation over the Bersimis River Basin, Quebec, a watershed where Hydro Quebec produces hydropower. Transfer functions developed during the WMO-SPICE experiment were applied to adjust Hydro-Québec's hourly precipitation amount at nine stations from 2010 to 2020. Since only solid precipitation needs to be adjusted, different phase partitioning methods were used, resulting in a total of 24 combinations of solid precipitation adjustment. Overall, the partitioning method using a sigmoidal transition obtained the most solid precipitation, whereas the -2°C threshold used by WMO-SPICE calculated the least amount of solid precipitation. As for the transfer functions, the Norwegian equations from Kochendorfer et al. (2017a ; 2017b) offered the largest solid precipitation corrections. The results strongly depend on wind speed as well as episodes of above 0°C temperatures during the cold season, where it is shown that the number of warm spells has a significant impact on the phase partitioning. The range of corrected solid precipitation during winter varies from an additional 15 to 100 mm depending on the equation and phase separation method chosen. The European Center for Medium-Range Weather Forecasts (ECMWF) Reanalysis v5 (ERA5) solid precipitations showed large variability when compared to the range of corrected solid precipitation. Overall, this study has shown that adjustments of the solid precipitation measurements over the Bersimis basin is needed to obtain a range of spring flood predictions to improve water management for hydrological power production.

Keywords: Wind undercatch, solid precipitation, phase partitioning.

2.1 Introduction

With climate change impacting precipitation patterns (Whitfield et al., 2020), properly monitoring precipitation throughout the year has become more and more crucial. The amount, phase, and spatial distribution of precipitation at the surface are the main inputs in hydrological models (Larson and Peck, 1974). Accuracy of hydrological models is critical because they provide information for flood forecasting, hydroelectricity production, as well as freshwater management all around the world (Cloke and Pappenberger, 2009 ; Devia et al., 2015 ; Larson and Peck, 1974). During the summer months, liquid precipitations dominate southern Quebec with sparse occurrence of hail that is not always captured by precipitation gauges. In contrast, falling precipitation measurements during fall, winter, and spring can be challenging because of undercatched solid precipitation caused by the wind as well as the determination of the phase of precipitation when precipitations occur near 0°C (Goodison et al., 1998 ; Rasmussen et al., 2001 ; Rasmussen et al., 2012).

Many measurement methods have been developed to measure snowfall, but all are associated with uncertainties (Groisman et al., 1991 ; Groisman and Legates, 1994 ; Goodison et al., 1998 ; Rasmussen et al. 2012 ; Yang et al., 1995). The types of measurement errors encountered can be categorized as evaporation losses, snow capping, blowing snow, and wind undercatch (Goodison et al., 1998). Kochendorfer (2015) showed that weighing gauges without anti-evaporating liquid can lose on average up to 0.12 mm h⁻¹ due to evaporation losses. Snow capping, defined as an accumulation of wet snow on the border of the entrance of the gauge, typically occurs when the perimeter of the orifice is not large enough (Rasmussen et al., 2012). This error can be solved by heating the orifice, thus melting the snow as it clusters the entrance (Rasmussen et al., 2001). Blowing snow can result in additional ground snow captured by the precipitation gauge and can become significant when a windshield is installed around the gauge (Rasmussen et al., 2012). Finally, wind undercatch is caused by the alteration of the flow around the gauge, resulting in particle being deviated away from the gauge (Thériault et al., 2012 ; Colli et al., 2015 ; Colli et al., 2016).

Wind undercatch cause solid precipitation underestimation of up to 50 % depending on the gauge type and climate conditions (Rasmussen et al., 2012 ; Yang et al., 1999). To reduce this wind effect, various types of shields are installed around the gauge. Largest shield further blocks the wind, and more precipitation will fall in the gauge. The Double Fence Intercomparison Reference (DFIR) with an automatic precipitation gauge is considered as the “true” measurements and is chosen as the reference to measure

solid precipitation (Goodison et al., 1998). As shown in Rasmussen et al. (2012), the DFIR and Small DFIR (SDFIR) measure the highest amounts of precipitation compared to the other precipitation gauges, even in the presence of strong winds.

To assess the gauge-shield configuration accuracy, the catch efficiency is often used. It is defined as the ratio between precipitation amounts measured by a gauge-shield system and the reference gauge-shield configuration (Wolff et al., 2015 ; Kochendorfer et al. 2017a ; 2017b). In general, as wind speed increases, the collection efficiency decreases, and a wide range of values are often measured at a given wind speed (e.g., Rasmussen et al., 2001 ; Thériault et al., 2012). The type of gauge only slightly influences the precipitation amounts compared to the shield (Kochendorfer et al., 2017b). The single-Alter (Alter, 1937) shield measures precipitation at wind speeds up to 5 m s^{-1} . At stronger wind speed, more than 50 % of the snow particles are deviated away from the gauge because of the strong updraft upstream (Thériault et al., 2012 ; Kochendorfer et al., 2017a).

To account for wind undercatch, transfer functions have been developed using the World Meteorological Organization's Solid Precipitation Intercomparison Experiment (WMO-SPICE) data (e.g., Kochendorfer et al., 2017a ; Wolff et al., 2015; Colli et al., 2020). Those transfer functions use the mean collection efficiency variation with wind speed. Kochendorfer et al. (2017a) developed various transfer functions based on the different WMO-SPICE sites that can be applied using different wind speed measurements available and 2-m temperature. The 2-m temperature is used to account for the phase of the precipitation. Applying these transfer functions to measured precipitation reduce the bias of solid precipitation measurements since they were developed on-site using referenced instruments (Goodison et al., 1998 ; Kochendorfer et al., 2017a ; 2017b ; Wolff et al., 2015 ; Colli et al., 2020).

The universal transfer function developed by WMO-SPICE combined various sites located in different climatic conditions. Sites are in the United States (US), Norway, and Canada. The particularities in the multiple transfer functions are visible within the coefficients, where qualitative analyses and Bayesian statistics were used to obtain them (Wolff et al., 2015). Depending on the differences between the precipitation gauge and the reference instrument, these coefficients vary. The Norway site is located in an alpine region and can reach up to 3 m of snow depth during winters (Kochendorfer et al., 2017a). This site is known for its strong winds, so undercatch is expected to be greater than the other sites (Kochendorfer et al., 2017a). The US site is located on the eastern slope of the Rocky Mountain in the Colorado Front

Range with grassland vegetation. Snow depth typically reaches less than 0.5 m over the course of winter for this site (Kochendorfer et al., 2017a).

The precipitation undercatch is also influenced by the phase and types of precipitation. Depending on the environmental conditions, liquid precipitation can exist at temperatures $< 0^{\circ}\text{C}$ and solid precipitation at temperatures $> 0^{\circ}\text{C}$ (Stewart et al., 2015 ; Harder and Pomeroy, 2013). To differentiate solid and liquid precipitation, Kochendorfer et al. (2017a ; 2017b ; 2018) assumed solid precipitation when temperatures are $< -2^{\circ}\text{C}$. Solid precipitation falls slower than liquid, so they are more affected by the wind speed, impacting the amount of precipitation falling in the gauge. Thériault et al. (2012) showed that the type of snow associated to the fall speed (Leroux et al., 2021) can influence the snow particle trajectory in the vicinity of the gauge. This can sometimes prevent snow to fall into the gauge, causing variability amongst the measured precipitation for a given wind speed. Finally, errors can appear in the recordings of precipitation, such as high-frequency noise, evaporation, effects of diurnal temperature, and mechanical and electrical interference can cause erroneous precipitation measurements from automatic recordings (Rasmussen et al., 2012 ; Ross et al., 2020). To reduce these errors, it is then essential to first filter the data before applying any precipitation partitioning or undercatchment correction.

Given the importance to accurately measure solid precipitation, the goal of this study is to characterize the ranges of solid precipitation measured when correcting for wind speed undercatch by using multiple phase partitioning methods. To do so, precipitation measurements and meteorological variables are used over the Bersimis river basin. Various wind undercatch methods developed with the WMO-SPICE data along with multiple phase partitioning methods are used to obtain a range of precipitation amounts over the river basin.

This paper will describe of the area of study as well as the instruments aboard the meteorological stations and the data used in section 2.2, followed by an overview of the experimental designs of multiple meteorological aspects. Section 2.3 will elaborate on wind speed, precipitation measurement, the different partitioning methods as well as the multiple transfer functions used. The results are presented in section 2.4. A discussion of the results and a comparison with reanalysis data are present in section 2.5. The conclusions are discussed in section 2.6.

2.2 Region of interest and datasets

2.2.1 Region of interest

The Bersimis watershed is in the Province of Quebec, Canada, and is home of two major hydroelectric power stations: Bersimis-1 (49°17'44.8"N 69°33'2.9"W) et Bersimis-2 (49°10'31"N, 69°13'45"W) (Figure 2.1). This basin represents an important source of forestry industry, hydroelectric energy, and recreational activities. The 16,000 km² watershed has a varying orography from 130 m to 1,000 m above sea level. From north to south, the basin is about 300 km long and is mostly located in boreal forests. There is a high variability in snowfall across the stations. Those hydroelectric power stations have an installed capacity of 1,178 MW for Bersimis-1 and 845 MW for Bersimis-2 (Hydro-Québec A, 1996-2022).

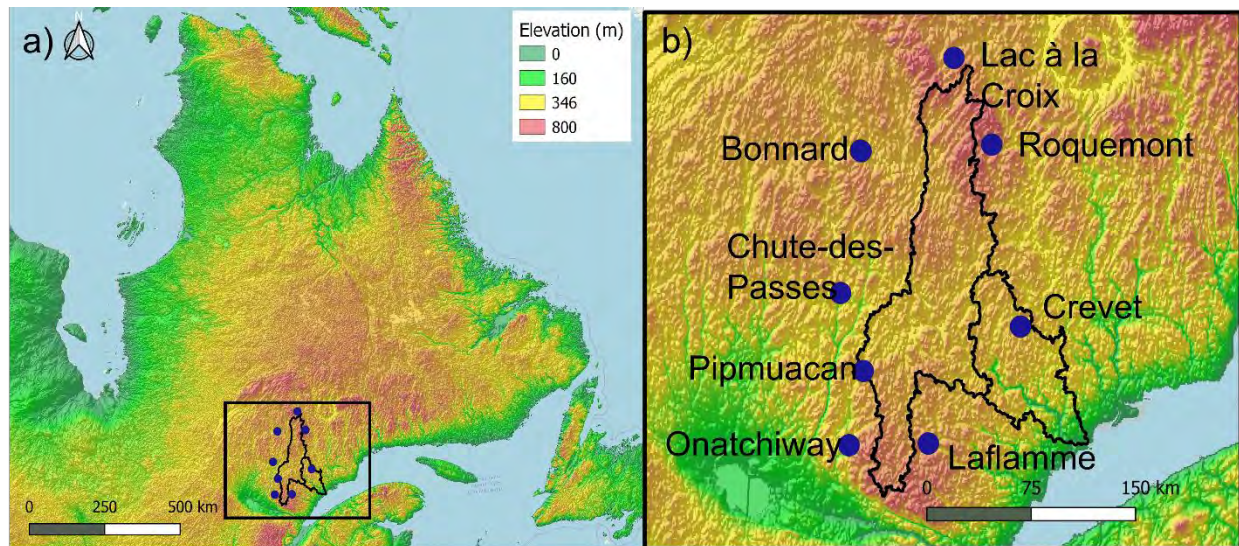


Figure 2.1 Map of the Bersimis River Basin located in Quebec, Canada. (a) is a larger view on the basin showing the hypsometry; (b) indicates the location and name of each station used in this study.

2.2.2 Datasets used

While data is available all year, only the data over the period of 1 October 2010 to 30 April 2020 is used in this study to focus on solid precipitation. There are multiple meteorological stations within the basin, but nine stations were chosen for this study (Figure 2.1), based on their data and instruments availability. These stations are called Lac à la Croix (APPENDIX A), Bonnard 1 and Bonnard 2, Chute-des-Passes, Pipmuacan, Laflamme, Crevet, Roquemont, and Manouane. These stations are maintained by many networks such as Hydro-Québec (HQ), Protection against forest fires Society (SOPFEU), Quebec Ministry

of Energy and Natural Resources (MERN), Environment and climate change Canada (EC) or the company Rio Tinto (RT). The elevation of the stations varies 303 m to 661 m (Table 2.1).

All the weather stations measure hourly standard meteorological variables such as temperature and humidity at 2 m above ground level, in addition to wind speed and direction at 10 m and occasionally 2.5 m above the ground. An all-weather OTT Pluvio² weighing gauge equipped with single-Alter shield at 2.5 m height above ground level. Since every site measure 10-m wind speed, the closest obstacles are 10 times their height distance from the anemometer according to the WMO (2006) standard. An example of a meteorological station is presented in Figure 2.2.

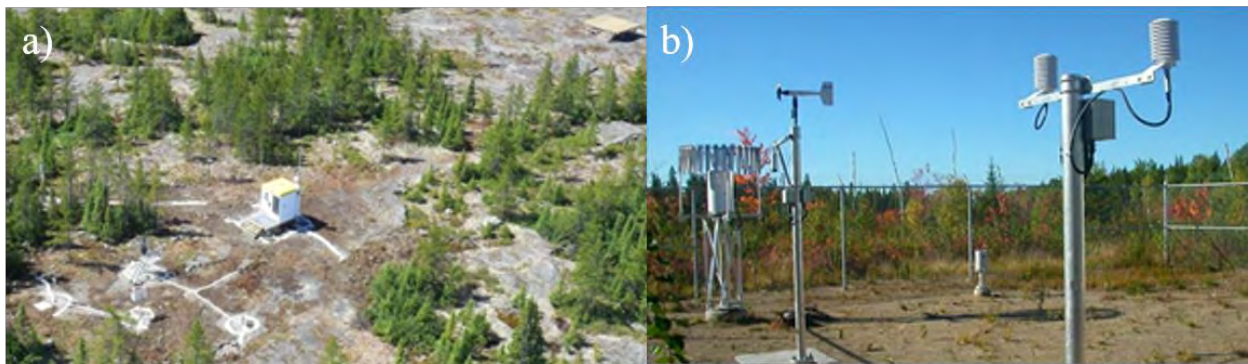


Figure 2.2: Example of a Hydro-Quebec weather station. (a) is the view from the top and (b) shows precipitation and meteorological instruments with 2.5-m wind speed only. Photo from Hydro-Quebec Production. 2-m temperature sensor, 2.5-m wind speed and wind direction sensor, precipitation gauge covered by single-Alter shield and rain gauge.

Table 2.1: The station used in this study. The longitude, latitude and site elevations are given. Hourly samples are the number of samples after applying the quality control procedure described in section 2.3.2.

Station	Longitude	Latitude	Site elevation [m]	Hourly samples
Lac à la Croix	51.3292	-70.0806	623	1317
Laflamme	48.9203	-70.2517	594	2394
Onatchiway	48.8942	-71.0317	303	3004
Crevet	49.6600	-69.3583	463	2261
Chute-des-Passes	49.8403	-71.1683	398	3319
Pipmuacan	49.3597	-70.9152	661	1241
Roquemont	50.7925	-69.6747	641	2415
Bonnard 1	50.7333	-71.0167	497	1673
Bonnard 2	50.7300	-71.0100	496	1678

2.3 Experimental design

2.3.1 Wind speed

Even though some stations measure wind speed at 2.5-m and 10-m, since the quality of the readings of wind speed at 2.5-m were not ideal, an estimation from Thom (1975) was used to obtain gauge height wind speeds derived from 10-m wind speeds at all sites. The wind speed at gauge height was estimated from the 10-m wind speed using the log-law wind profile, with a displacement height of 0.4 m and a roughness length of 0.01 m, as in Kochendorfer et al. (2017a). The displacement height is known as the height at which the logarithm of the wind profile is subjected to be zero and the roughness length expresses the roughness of the surface.

2.3.2 Precipitation measurements

A quality control was applied on the hourly precipitation measurements. To detect and filter data quality errors such as frequency noise, evaporation and more, the segmented neutral aggregating filter (NAF-SEG), an automated filtering method, proposed by Ross et al. (2020), was applied to the raw cumulative precipitation data. First, this filtering method corrects the noise from cumulative precipitation data and considers the diurnal oscillations in the bucket weight signal (Smith et al., 2019). The total cumulated precipitation remains unchanged from the initial raw sum of precipitations. Secondly, this method corrects for evaporative losses. Measurement errors due to evaporation can lead up to 10 % (Ross et al., 2020). This method used three 24-h overlapping moving windows advanced by 8-h increments. A more detailed description of the method is given in Ross et al. (2020). The remaining errors were removed by ensuring that the cumulated precipitation amount is always smaller than the amount at the next timestep using a rolling maximum filter as in Harder and Pomeroy (2013).

After filtering and removing certain biased periods, a recommended precipitation threshold was applied to the raw data following the Kochendorfer et al. (2017a, 2017b) method. A minimum of 0.25 mm per 30 minutes reading was imposed to limit the errors associated with small values under Kochendorfer et al. (2017a) recommendations. Since the data used in this study uses 1-h recordings, the minimum threshold was converted to 0.5 mm. A last threshold of hourly precipitation was applied to remove values over 10 mm h⁻¹ since they were determined to be unrealistic values during winter. Depending on the stations, some technical difficulties were apparent, and no filtering method could recover the data. To ensure the quality of the results, those erroneous periods were removed. At total of 19,302 hourly samples although remained for all 9 sites combined (Table 2.1). As for the missing hourly data, they were not used in this

study. The years 2013 to 2017 and 2019 were removed for Pipmuacan, 2014 was removed for Roquemont, 2015 to 2017 and 2019 were removed for Lac à la Croix, 2015 and 2019 were removed for Onatchiway and 2011 was removed for Crevet. Bonnard 1 and 2, Laflamme and Chute-des-Passes have data for the 10 winters.

2.3.3 Phase partitioning method

Transfer functions developed for mixed precipitation were applied at all 2-m air temperature. In contrast, the transfer functions developed for solid precipitation should be used only when the temperature is $< -2^{\circ}\text{C}$ (Kochendorfer et al., 2017a ; 2017b) or when solid precipitation is found. Therefore, four different precipitation phase partitioning methods were chosen and are summarized in Figure 2.3. Static air temperature thresholds, as well as a linear variation of temperature (Quick and Pipes, 1997) referred as PQ in this paper, and a sigmoidal temperature variation (Kienzle, 2008) were used. Static threshold temperature methods have been commonly applied in various studies (e.g. Kochendorfer et al., 2017a ; 2017b), as well as in hydrological and snow models (e.g. Quéno et al., 2018 ; Marks et al., 2013). These methods separate precipitation into 100% solid precipitation when temperatures are below the threshold temperature, otherwise 100% liquid precipitation is assumed. In this study, two static thresholds were used: 1) 0°C because it is the temperature at which solid precipitation will melt in saturated conditions; 2) -2°C because it is the temperature used by WMO-SPICE. Two other partitioning methods with a varying fraction of solid and liquid precipitations were tested: PQ with a linear transition between 2°C and -2°C and Kienzle with a sigmoidal transition 8°C and -4°C . See APPENDIX B for details of the PQ and Kienzle partitioning methods.

These partitioning methods were selected to analyze the relative accumulation of rain and solid precipitation. The measured relative humidity during precipitation for each site varied between 85% and 92% on average. Since the relative humidity was high, the precipitation phase was only estimated using the air temperature. When the temperature is $< -4^{\circ}\text{C}$, no liquid precipitation is formed by any methods (Figure 2.3). When the temperature is between 2°C and 8°C , dispersion amongst the Kienzle partition and the three other methods can be seen. As the air temperature is $> 0^{\circ}\text{C}$, the PQ method deviates from the T0 and T2 methods. Hence, the amount of liquid precipitation increases as the average temperature rises.

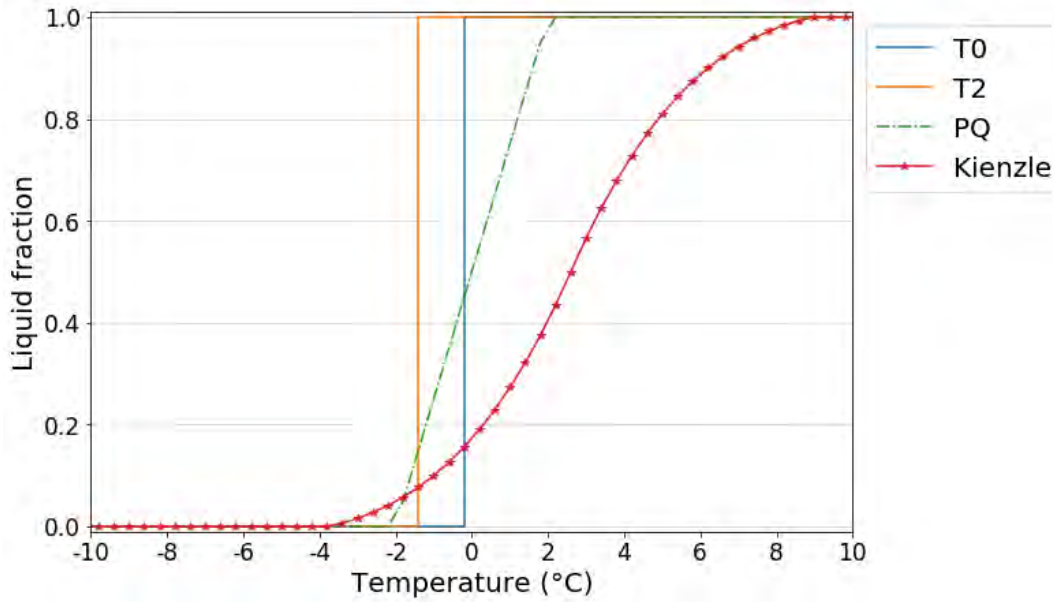


Figure 2.3: Liquid fraction estimated by four different partitioning methods using temperature ranging from -10°C to 10°C. T0 represents the T = 0°C threshold, T2 represents the T = -2°C threshold, PQ represents the PQ linear threshold and Kienzle represents the Kienzle sigmoidal threshold.

2.3.4 Transfer functions

Three forms of transfer functions were used in this study to estimate the collection efficiency of weighing precipitation gauges in single-Alder shields. The first transfer function estimates the collection efficiency (CE) as a function of only wind speed (Equation 2.1, Kochendorfer et al., 2017a ; 2017b), the second depends on both wind speed and air temperature (Equation 2.2, Kochendorfer et al, 2017a ; 2017b), and the third varies with both wind speed and precipitation intensity (Equation 2.3, Colli et al., 2020).

$$CE = a e^{-bU} + c \quad (2.1)$$

$$CE = e^{-aU} (1 - [\tan^{-1} (b T) + c]) \quad (2.2)$$

$$CE = e^{-aU} (1 - [\tan^{-1} (b SI) + c]) \quad (2.3)$$

where CE is the collection efficiency, a, b and c are the parameters given in Table 2.2, U is either the 2.5-m or 10-m wind speed ($m s^{-1}$), T is the 2-m air temperature (°C) and SI is the snowfall intensity.

Different coefficients for these transfer functions exist and depend on different geographic areas (e.g. Smith et al., 2020 ; Kochendorfer et al., 2017a ; 2017b ; 2018 ; Wolff et al., 2015). For instance,

Kochendorfer et al. (2017a) has different coefficients obtained at the Norwegian site (NOR10 and NOR2), than the United States of America’s site (USA10 and USA2) or even the combination of both locations (All10 and All2). The a, b and c coefficients are all associated with different winter climates (Kochendorfer et al., 2017b). The different sets of coefficients evaluated at our sites and acronyms are presented in Table 2.2 below. For these transfer functions, thresholds in wind speed were applied as in Kochendorfer et al. (2017a), for instance, for some transfer functions, wind speeds above 9 m s^{-1} and 7.2 m s^{-1} at 10 m and 2 m, respectively, remained the same as the threshold value. This was established to avoid over precipitation correction, which was shown to accurately correct the precipitation measurements (Kochendorfer et al., 2017b).

Table 2.2: Transfer functions used to correct for precipitation wind undercatch (Kochendorfer et al., 2017a, 2017b and Colli et al., 2020). The wind speed is in m s^{-1} and the air temperature is $^{\circ}\text{C}$.

Acronyms	Description	Reference
USA2	2-m wind speed, 2-m air temperature. Coefficients obtained based on measurements made by the Single Alter (SA) shielded gauge at the Marshall (US) test site from 1 January 2009 to 7 March 2014, and include all seasons. Coefficient values: $a = 0.036$, $b = 1.04$, $c = -0.63$. Referred to equation 2.2.	Kochendorfer et al., 2017a
USA10	10-m wind speed, 2-m air temperature. Coefficient values: $a = 0.030$, $b = 1.06$, $c = -0.63$. Referred to equation 2.2.	
NOR2	2-m wind speed, 2-m air temperature. Coefficients obtained based on measurements made by the Single Alter (SA) shielded gauge at Haukeliseter, Norway (NOR) test site from 1 February–30 April 2011; 1 November 2011–30 April 2012, and 1 February–31 May 2013. Coefficient values: $a = 0.054$, $b = 0.71$, $c = -0.26$. Referred to equation 2.2.	
NOR10	10-m wind speed, 2-m air temperature. Coefficient values: $a = 0.050$, $b = 0.66$, $c = -0.23$. Referred to equation 2.2.	
All2	2-m wind speed, 2-m air temperature. Coefficients obtained from the combination of USA and Norway. Coefficient values: $a = 0.040$, $b = 1.10$, $c = -0.54$. Referred to equation 2.2.	
All10	10-m wind speed, 2-m air temperature. Coefficient values: $a = 0.030$, $b = 1.04$, $c = -0.57$. Referred to equation 2.2.	
U2	2-m wind speed only. Coefficient values: $a = 0.728$, $b = 0.230$, $c = 0.336$. Referred to equation 2.1.	Kochendorfer et al., 2017b
U10	10-m wind speed only. Coefficient values: $a = 0.742$, $b = 0.181$, $c = 0.322$. Referred to equation 2.1.	
UT2	2-m wind speed, 2-m air temperature. Coefficient values: $a = 0.0348$, $b = 1.366$, $c = -0.779$. Referred to equation 2.2.	
UT10	10-m wind speed, 2-m air temperature. Coefficient values: $a = 0.0281$, $b = 1.628$, $c = -0.837$. Referred to equation 2.2.	

NOR2_T	2-m wind speed and 2-m air temperature	Coefficient values: a = 0.1713, b = 0.0767, c = -0.0579. Referred to equation 2.2.	Colli et al., 2020
NOR2_SI		Coefficient values: a = 0.5557, b = 11.0022, c = -0.7073. Referred to equation 2.3.	
CAN2_T		Coefficients obtained based on measurements made by the Single Alter (SA) shielded gauge at the CARE (Canada) test site from October 2013 to April 2015. Coefficient values: a = 0.3103, b = 0.0116, c = 0.7711. Referred to equation 2.2.	
CAN2_SI		Coefficients obtained based on measurements made by the Single Alter (SA) shielded gauge at the CARE (Canada) test site from October 2013 to April 2015. Coefficient values: a = 12.5937, b = 338.0402, c = -0.5737. Referred to equation 2.3.	
USA2_T		Coefficients obtained based on measurements made by the Single Alter (SA) shielded gauge at the Marshall (US) test site from October 2013 to April 2015. Coefficient values a = 0.0560, b = 0.2148, c = -0.8542. Referred to equation 2.2.	
USA2_SI		Coefficients obtained based on measurements made by the Single Alter (SA) shielded gauge at the Marshall (US) test site from October 2013 to April 2015. Coefficient values a = 0.4156, b = 8.7795, c = -0.7062. Referred to equation 2.3.	

2.3.5 Data analysis

First, the temperature and precipitation climatology of the stations were analyzed. This step was essential to identify the differences between the stations and how these can affect the performance of the transfer functions, hence the amount of solid precipitation corrected. Second, the amount of liquid and solid precipitation estimated from the different partitioning methods was evaluated. Third, the different transfer functions were compared amongst them by correcting solid precipitation using -2°C as the threshold for solid precipitation occurrence same as proposed by WMO-SPICE. Six transfer functions were selected amongst the 16 equations since redundancy in the results using different transfer functions were detected (section 2.4.3). Finally, the combined results of both the partitioning methods and the six transfer functions were compared with reanalysis data to evaluate the added value of corrected precipitation amounts. In this study, reanalysis data will be considered as the reference for solid precipitation amounts.

The various transfer functions summarized in Table 2.2 are shown in Figure 2.4. The collection efficiency decreases with increasing wind speed. Up to 50% difference in CE is found for wind speed of 7 m s^{-1} . Most

of the transfer functions are within 30% CE at wind speed $> 5 \text{ m s}^{-1}$. The 16 equations chosen are indicated in Figure 2.4.

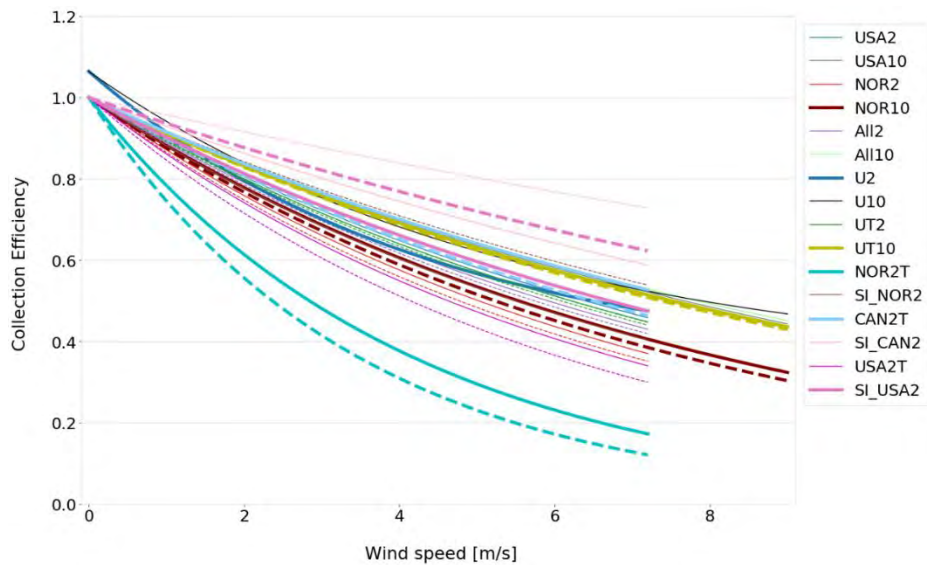


Figure 2.4: The collection efficiency (CE) of each transfer function as a function of wind speed, gauge height and 10-m wind speed combined. For equations dependent of air temperature, the solid lines modelling CE with respect to wind speed, represent $T = -5^{\circ}\text{C}$ and the dotted lines represent $T = -10^{\circ}\text{C}$. For the equations dependent on snowfall intensity (SI), the solid lines modelling CE, with respect to wind speed, using $\text{SI} = 1 \text{ mm h}^{-1}$ and for the dotted lines, $\text{SI} = 5 \text{ mm h}^{-1}$ (Kochendorfer et al., 2017b). The acronyms are given in Table 2.2.

2.4 Results

2.4.1 Climatology

The precipitation, wind speed and temperature climatology are presented in this section. The analysis focuses on 1 October to 30 April period from 2010 to 2020.

2.4.1.1 Precipitation

The total annual precipitation amount measured during each winter for all nine sites is presented in Figure 2.5. Chute-des-Passes (CDP) and Onatchiway received the highest precipitation amount over the 10 winters, with 4,968 mm and 4,791 mm, respectively. In contrast, Lac à la Croix (Croix) and Pipmuacan received the lowest precipitation amount (1,988 mm and 1,858 mm, respectively). Bonnard 1 and 2 have similar precipitation climatology, with 2,514 mm and 2,531 mm total for the 10 winters, respectively. Except for 2010, and 2012, those two stations recorded the lowest precipitation amount per winter season. Overall, on average per year, the stations with highest and lowest total precipitation remain consistent

throughout the years. The stations with the highest annual recorded precipitation occurrence are Onatchiway, followed by Chute-des-Passes. The annual accumulated precipitation from of October to April ranged from 200 mm to 600 mm, depending on the stations.

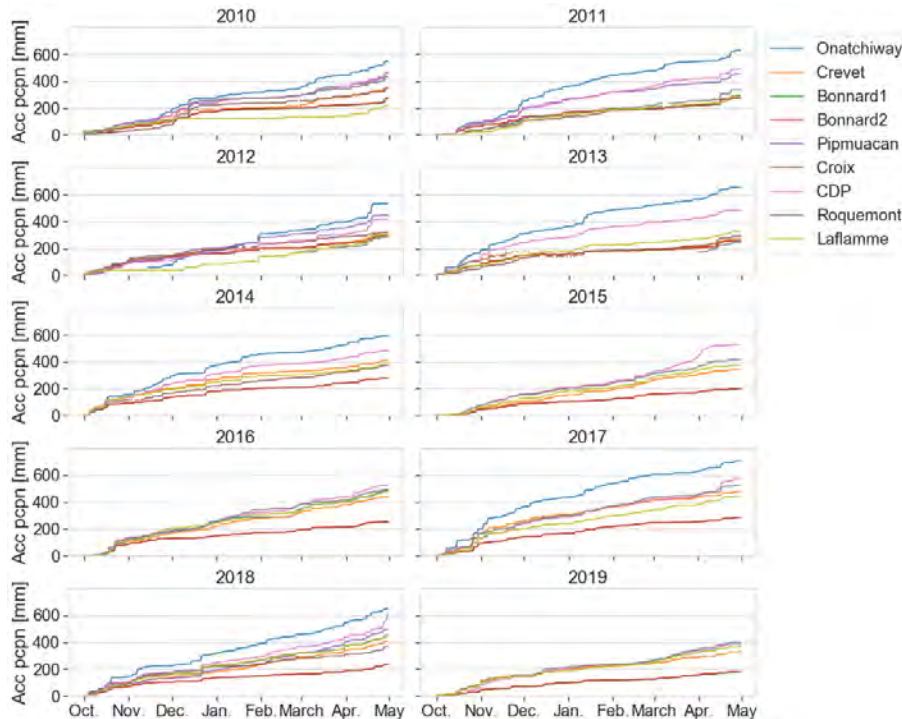


Figure 2.5: Yearly cumulated total precipitation [mm] for all 9 sites from October 2010 to April 2020. Croix and CDP are Lac à la Croix and Chute-des-Passes, respectively. Since Bonnard 1 and 2 have similar accumulated precipitations, only Bonnard 2 is visible.

2.4.1.2 Wind speed

The distribution of 10-m wind speed values at all sites are shown in Figure 2.6. At all sites, 10-m wind speed is mainly $< 5 \text{ m s}^{-1}$, with some site-to-site variability. For example, Laflamme, Bonnard 1, and Bonnard 2 measured the strongest wind speed, that reached up to $> 10 \text{ m s}^{-1}$. These strong wind speeds are probably due to the location of the stations; Laflamme is in the bottom of a valley along the riverbank, and Bonnard 1 and 2 are in open fields near a body of water. A similar behaviour was observed for the 2-m wind speed (Figure 2.7) since they are directly correlated to the 10-m wind speed from the log-law wind profile (Thom, 1975). However, the use and illustration of both 2-m and 10-m wind speed measurements are necessary since their impact on solid precipitation is different for equal wind speeds, meaning the impact of a wind speed of 5 m s^{-1} measured at 2 m is not the same as a 5 m s^{-1} wind speed measured at 10 m.

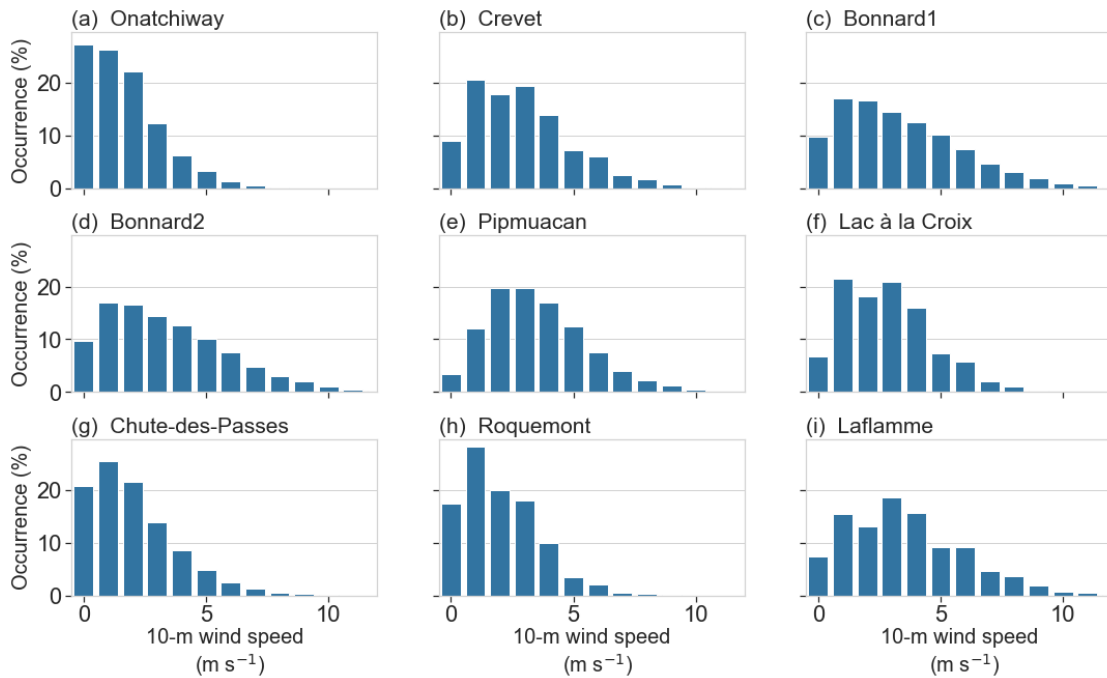


Figure 2.6: Percentage of occurrence of the 10-m wind speed at each station during the winter months from 1 October 2010 to 30 April 2020. The location of the stations is given Figure 1. Wind speed bins used are 1 m s^{-1} .

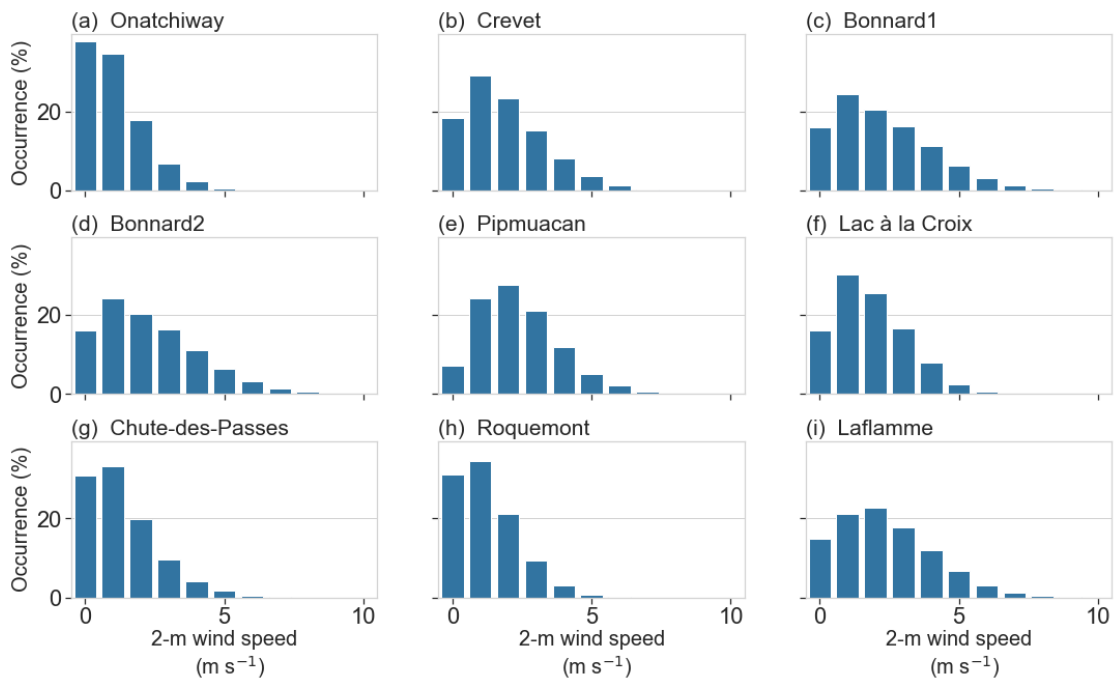


Figure 2.7: Percentage of occurrence of the 2-m wind speed at each station during the winter months from 1 October 2010 to 30 April 2020. The location of the stations is given Figure 1. Wind speed bins used are 1 m s^{-1} .

2.4.1.3 Air temperature

From 1 October to 30 April, the mean hourly 2-m air temperature at all sites was below 0°C (Figure 2.8). Temperatures near -40°C were measured at least once at all sites. The peak frequency in the temperature was between -2°C and 2°C at six sites; at the remaining sites, it was the second most common temperature interval. This was also observed reported in Mekis et al. (2020) at locations across Canada. Events with temperatures between -2°C and 2°C are referred to as warm spells as snowfall and mixed precipitation are commonly observed within this range of surface temperature (Nitu et al., 2019).

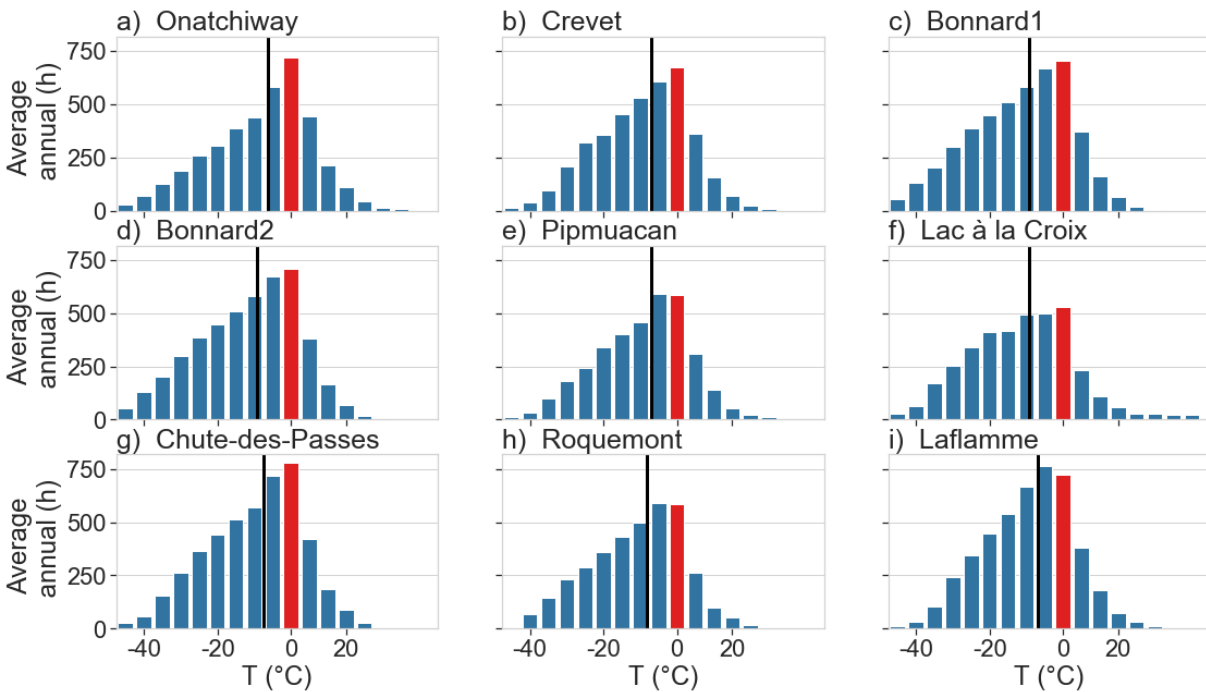


Figure 2.8: Annual average number of hours for different temperature bins (bins of 4°C) for each station. The red bar highlights the temperature between -2°C and 2°C and the black vertical bar shows the mean temperature at each station over the whole period.

The monthly occurrence of warm spells varies amongst sites (Figure 2.9). Most of these warm spells occurred during the shoulder months such as October, November, and April. Most stations measured similar monthly warm spells occurrences with some variation. Pipmuacan and Lac à la Croix sites stand out because they have the smallest amounts of winter years after the quality control filtering. The lowest

amounts of warm spells, in turn, are measured at those sites. Chute-des-Passes experienced the highest number of warm spells in December to April, closely followed by Laflamme.

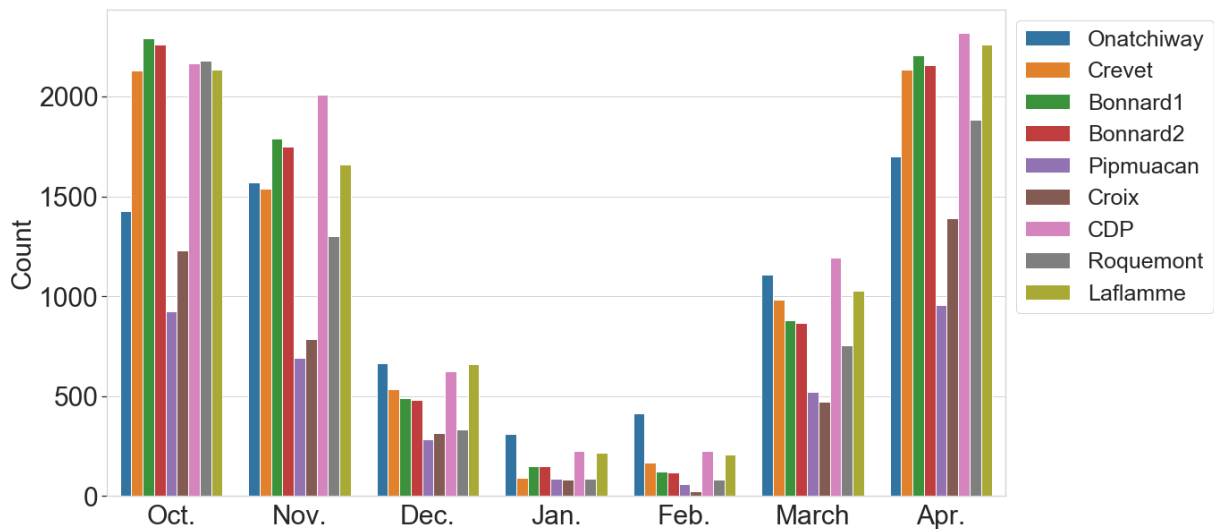


Figure 2.9: Number of warm spells (temperature between -2°C and 2°C) per month for each station from 2010 to 2020. Croix represents Lac à la Croix and CDP represents Chute-des-Passes.

The occurrence of warm spells varies greatly annually across the river basin (Figure 2.10). The lowest number of warm spells and the less inter-annual variations occurred at Lac à la Croix, while Onatchiway and Chute-des-Passes measured at least 2 years of more than 1,000 occurrences of warm spells. At most stations, the mean accumulated number of warm spells was between 500 and 1,000 per month. Furthermore, most stations measured very few events during the coldest months, but the duration of this flat slope varies annually. For example, Bonnard 1 and 2 measured very little warm spells in 2013 during winter (December to – February) but many of them in 2010, spans from November to March.

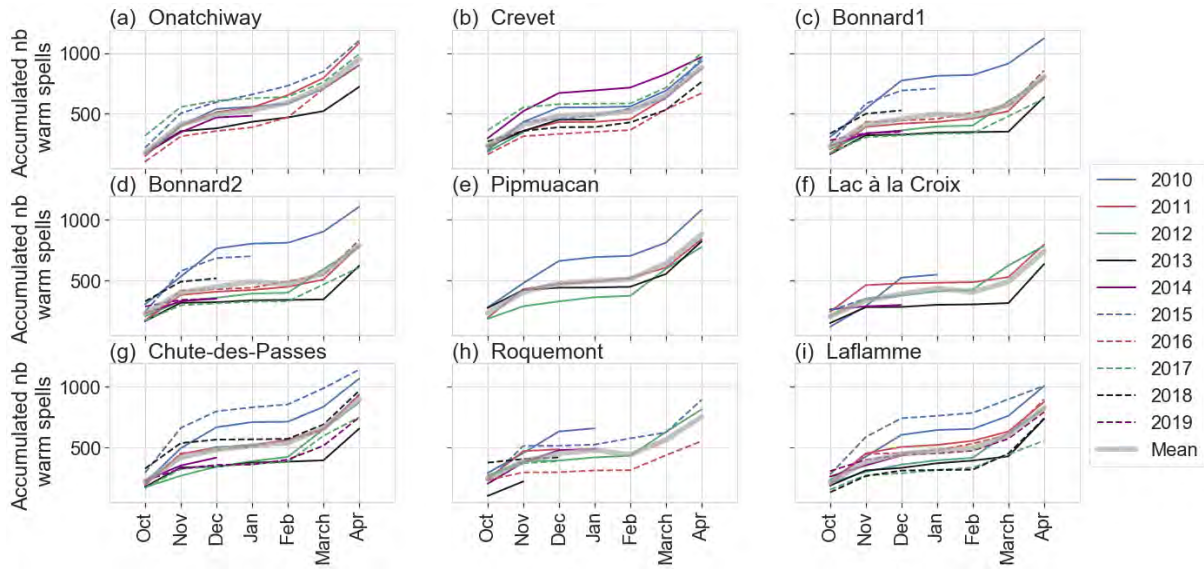


Figure 2.10: Annual accumulated number of warm spells per month over each hydrological year (October of the written year up to April of the next year) for each station (temperature between -2°C and 2°C).

2.4.2 Phase partitioning

Given the occurrence of warm spells shown previously, it is necessary to investigate various phase partitioning methods to identify the amount of solid precipitation that should be corrected with the transfer function. The estimated percentages of solid precipitation from the different phase partitioning methods are evaluated (Figure 2.11). The methods used are given in Figure 2.3. All stations were combined to conduct an annual and monthly evaluation (Figure 2.11). First, the relative amount of snow varied annually. The method using the static threshold at -2°C (T2) always estimated the lowest amount of solid precipitation, which this is the threshold proposed by WMO-SPICE (Kochendorfer et al., 2017a). T0 and PQ performed similarly and estimated that solid precipitation was between 30% to 80% of total amount each year. In contrast, Kienzle estimated the highest amount of solid precipitation, with above 60% of the total amount during most years. Second, for PQ, T0 and T2, the monthly occurrence shown in Figure 2.11 b), indicates a wider range of values during November and April compared to the other months. Kienzle has the narrowest monthly range, as well as on an annual basis, excluding 2011 and 2012. The monthly variation shows that the phase partitioning methods differ significantly during the fall and spring.

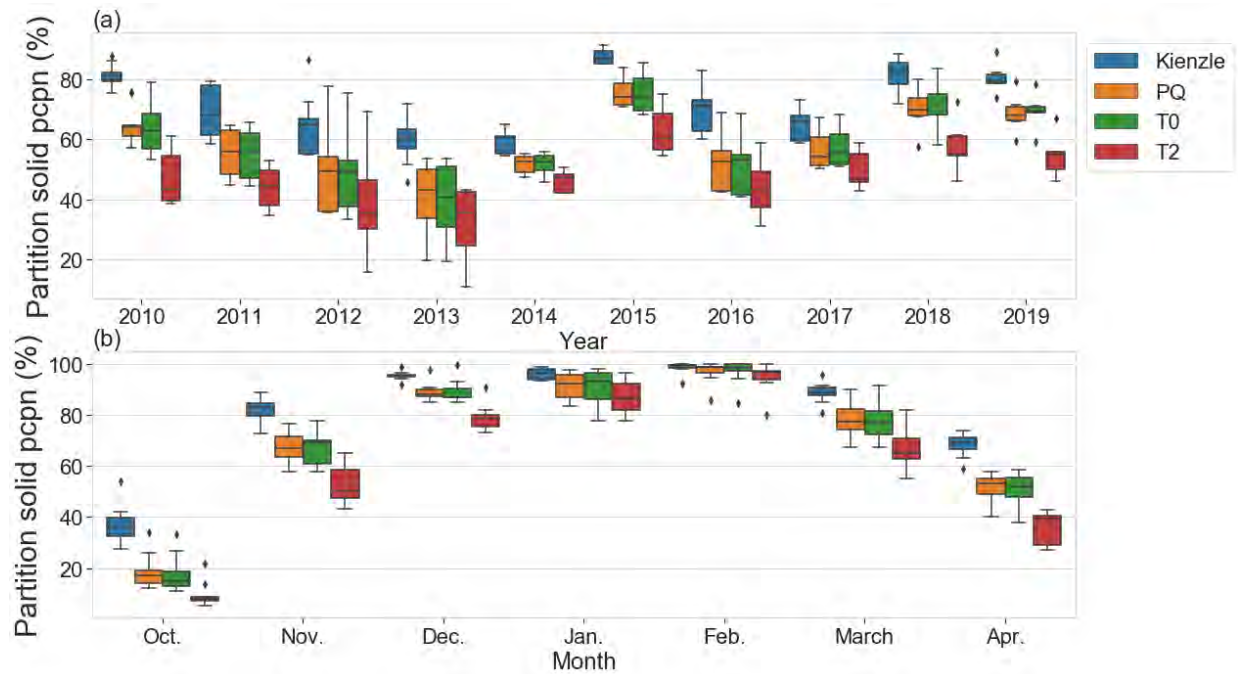


Figure 2.11: Percentage of snow for all station data for the three different partitioning methods (a) per hydrological year (e.g. 2010 is from October 2010 to April 2011) and (b) per month. The different partitioning methods are identified as T0 for the static threshold at $T = 0^{\circ}\text{C}$, T2 as the $T = -2^{\circ}\text{C}$ static threshold, PQ represents the linear transition method by Quick and Pipes (1977) and Kienzle represents the sigmoidal transition.

The total amount of liquid and solid precipitation estimated by each phase partitioning method for all the stations are shown in Figure 2.12. The T0 method produced similar amounts of solid precipitation as PQ, with solid cumulated precipitation always higher than the liquid. The solid precipitation amount was usually between the T2 and Kienzle, where T2 produced the lowest amount of solid precipitation and Kienzle the highest. Finally, Onatchiway and Bonnard 1 and 2 are the only stations that received less solid precipitation amount than liquid precipitation using T2.

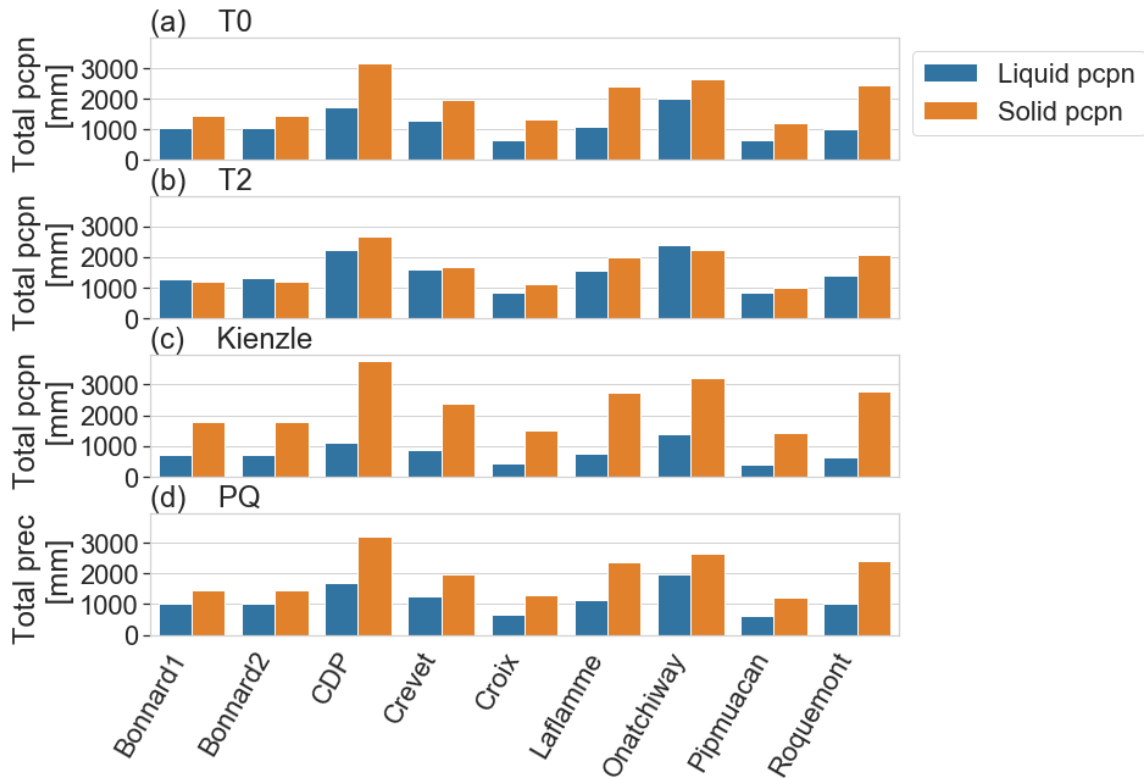


Figure 2.12: Total accumulated liquid and solid precipitation (blue and orange, respectively) for a) partitioning method is 0°C or below, b) partitioning method solid when temperature is -2°C or below, c) Kienzle sigmoidal partitioning method (Kienzle, 2008) and d) Quick and Pipes (1977) partitioning method for each station over 10 years for warm spells (temperature between -2°C and 2°C). Croix represents Lac à la Croix and CDP represents Chute-des-Passes. Note that due to the filtering method and requirements needed to apply the transfer functions, the number of hourly samples differ for each site (Table 2.1).

2.4.3 Corrected precipitation using various transfer functions

The performance of the different transfer functions during a 10-winter period is shown in Figure 2.13. The T2 method was chosen for the comparison of the different results obtained by the transfer functions since this method was chosen as the threshold in Kochendorfer and al. (2017a ; 2017b). Chute-des-Passes (CDP) and Onatchiway recorded the highest measured solid precipitation over the 10 winters using T2, whereas Lac à la Croix (Croix), Pimtuacan, Bonnard 1 and 2 recorded the lowest accumulations (Figure 2.13a). When looking at the corrected solid precipitation amounts, we noticed that Laflamme has higher values than Onatchiway while they were associated with lower amounts of solid precipitation initially. The corrected precipitation using 10-m wind speed transfer functions estimated the highest accumulated solid precipitation over the 10 winter years using NOR10 (Table 2.2) for all sites. As for the 2-m wind speed transfer functions, CAN2_T followed by NOR2_T estimated the highest solid precipitation accumulations.

USA2_SI is the equation that estimated the lowest amount of solid precipitation. All the other transfer functions estimated a range of comparable values, producing similar results.

To distinguish the different equations over the entire dataset, the mean annual difference between the annual sum of corrected solid precipitation with the measured annual sum was calculated for each station for all 16 equations based on the measured solid precipitation using the T2 partitioning method (Figure 2.13b). The mean bias for most of the sites ranges around 15 to 100 mm y⁻¹. Laflamme and Pipmuacan have higher mean bias than the other sites, with Pipmuacan ranging from to 41 to 239 mm y⁻¹.

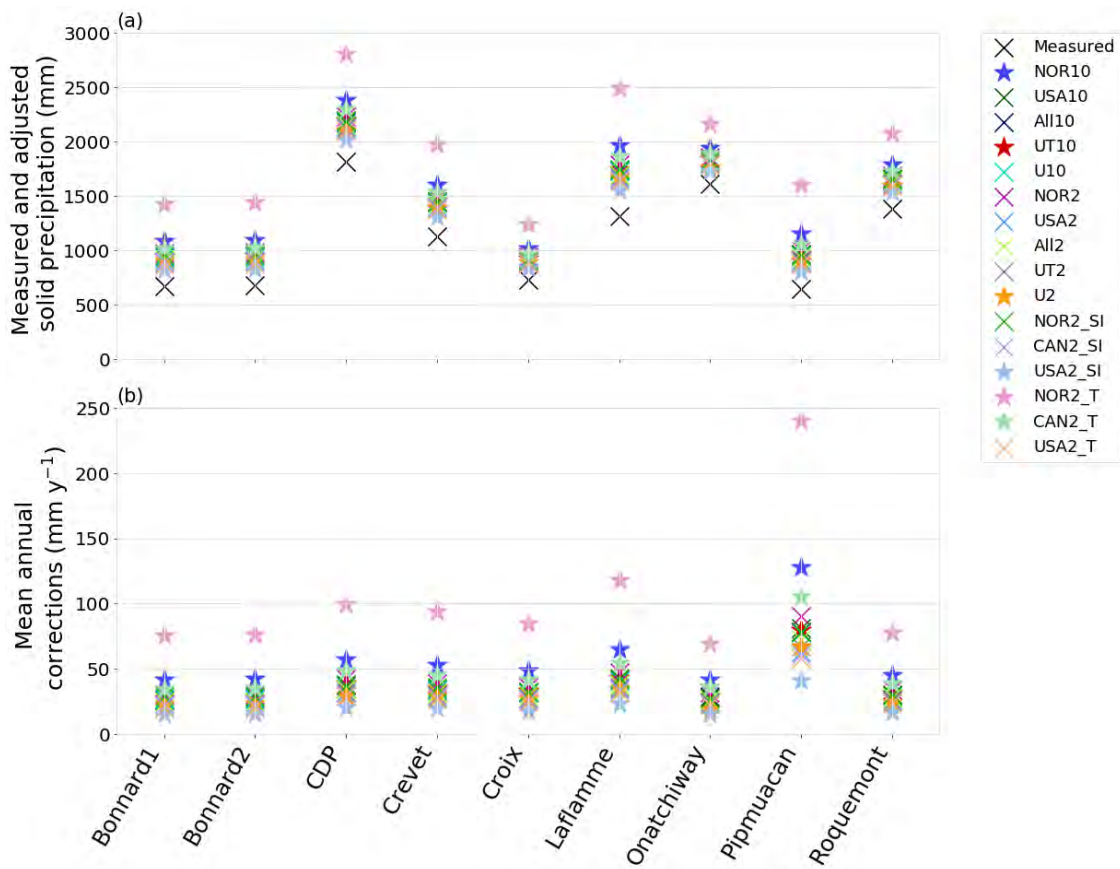


Figure 2.13: (a) Measured and adjusted accumulated solid precipitation from 1 October 2010 to 30 April 2020, at each station. Solid precipitation is assumed to be at 0°C (T0) and 16 transfer functions were used. (b) Mean annual corrections (mm y⁻¹) from 1 October 2010 to 30 April 2020 per station for the 16 transfer functions. Acronyms shown in the legend are defined in Table 2.2. Croix represents Lac à la Croix and CDP represents Chute-des-Passes.

Table 2.3 summarizes the mean corrections obtained for every transfer function at Chute-des-Passes. Chute-des-Passes was chosen because it reported the maximum amount of solid precipitation amongst other stations. The transfer functions were classified into six categories regrouping similar corrections.

First, All10, USA10, NOR2, UT10 and U10 (group A) all have similar bias (~120.4), giving overall similar correction factors. The second group (B) sorted as All2, USA2, UT2, CAN2_SI, NOR2_SI, USA2_T and U2 also have similar bias (~116.7). For the remaining groups, no similarities were identified amongst the equations, hence their behaviour is unique and requires further analysis. Then, we selected one equation for each group to eliminate repetition amongst the results. For the group A, the universal transfer function, UT10, was selected and CAN2_SI for group B. Since all the other groups contained one equation, groups C to F were kept for the analysis. Therefore, six equations are used for the remaining of the analysis. These are UT10, NOR10, CAN2_T, NOR2_T, U2 and USA2_SI. These allow a range of corrected precipitation, from different climate conditions and two wind speed levels as well as using the snowfall intensity. The selected equations are marked in bold in Figure 2.4 and represented by stars in Figure 2.13.

Table 2.3: Annual mean bias percentage for Chute-des-Passes station using the T2 threshold method for winter years of 2010 to 2020. Equations are classified in various groups from A to F. The classification was grouped by similarity in bias values.

Equation	Bias (%)	Group
NOR10	130.3	E
All10	119.8	A
USA10	120.3	A
NOR2	122.5	A
All2	118.5	B
USA2	116.9	B
UT10	120.7	A
UT2	117.4	B
CAN2_SI	116.2	B
CAN2_T	125.9	D
NOR2_SI	120.3	A
NOR2_T	152.4	F
USA2_SI	111.2	C
USA2_T	115.7	B
U10	118.7	A
U2	115.6	B

2.4.4 Phase partitioning use various methods and corrected solid precipitation amounts

Six different equations were identified to analyze the variability of accumulated solid precipitation over the river basin. Figure 2.14 shows total precipitation amounts estimated by the different transfer functions. As observed in Figure 2.12, the partitioning method with the highest amount of solid

precipitation is Kienzle, followed by PQ and T0 methods. The method with the lowest solid precipitation amount is T2. Regarding the corrected solid precipitation amounts per station and method, the equation with the highest correction for the 10-m wind speed is NOR10, and for the 2-m wind speed, NOR2_T, closely followed by CAN2_T. Overall, the different transfer functions behaved similarly for the different phase partitioning methods, except for the Kienzle and PQ methods. Indeed, CAN2_T estimated more than NOR2_T. The partitioning methods were similar, where NOR2_T and USA2_SI estimated more and less precipitation than the other transfer functions, respectively. The results are consistent throughout the different partitioning methods and corrected solid precipitation measurements. In other words, the partitioning methods set the initial amount of solid precipitation to be corrected, and depending on the impact of temperature and wind, wind only or temperature and snowfall intensity, the corrected amount is added to the initial solid precipitation amount with the use of the transfer functions.

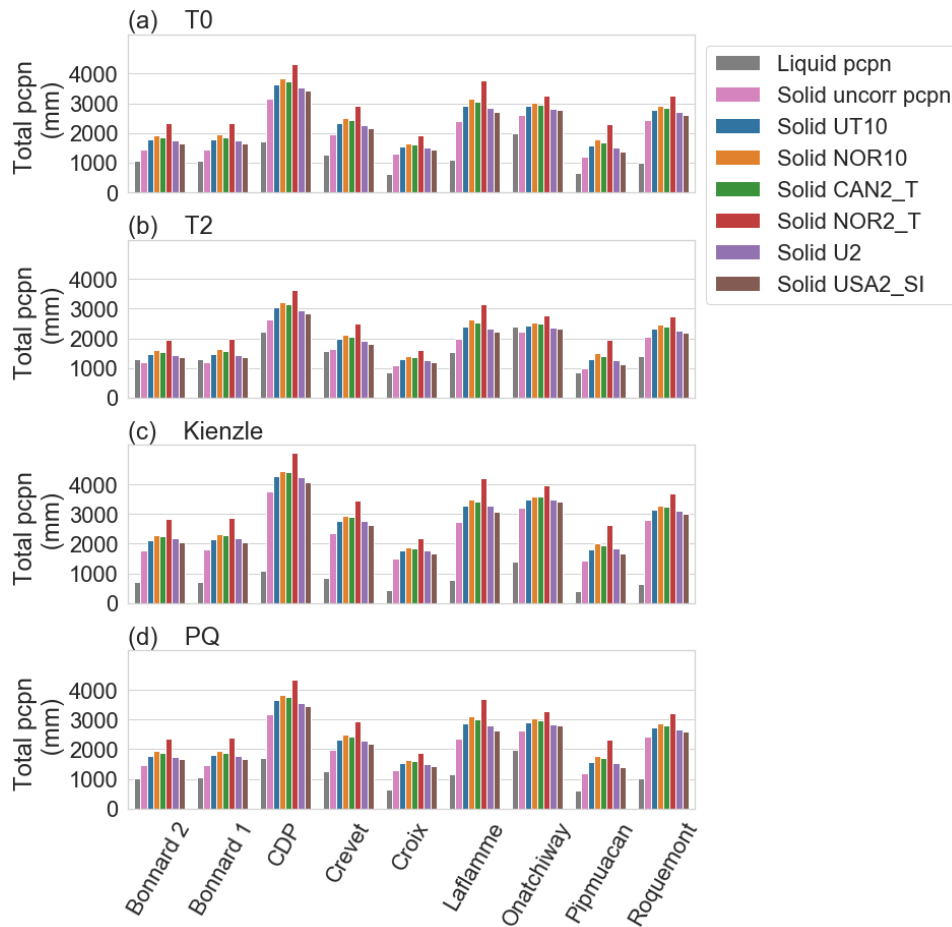


Figure 2.14: Total amount of precipitation (mm) from 2010 to 2020 for the months of October to April for each station for the different phase partitioning methods. a) partitioning method is 0°C or below, b) partitioning method solid

when temperature is -2°C or below, c) Kienzle sigmoidal partitioning method (Kienzle, 2008) and d) Quick and Pipes (1977) partitioning method.

Since the wind speed is responsible of the precipitation undercatch, the corrections are evaluated in function of their respective wind speeds. The relationship between the measured and corrected accumulations with 2-m wind speed (U) bins are illustrated in Figure 2.15. Most of the precipitations occur at wind speeds between 0 to 3 m s^{-1} at the 9 sites. Pipmuacan has similar amounts of additional solid precipitations at wind speeds between 0 to 3 m s^{-1} wind speed than at 3 to 6 m s^{-1} . We notice that even though the measured quantity is lower at wind speed between 3 to 6 m s^{-1} , the corrected amount suggested by the NOR2_T transfer function is close to the corrected amounts at lower wind speeds, even with more precipitation measured initially. As for U2 and USA2_SI at Pipmuacan at 3 to 6 m s^{-1} , these corrections do not offer as much additional snow than when the wind speed is lower. Lower precipitation amounts occur at higher wind speed for all sites. Only Laflamme, Pipmuacan, Bonnard 1, Bonnard 2 and Chute-des-Passes recorded some precipitation when the wind speed is $> 6 \text{ m s}^{-1}$. Corrected amounts of solid precipitation with NOR2_T produced systematically the highest amount of precipitation, while USA2_SI produced the lowest. This phenomenon can be explained by the characteristics of the WMO-SPICE sites used to derive the coefficients of the equations (Wolff et al., 2015).

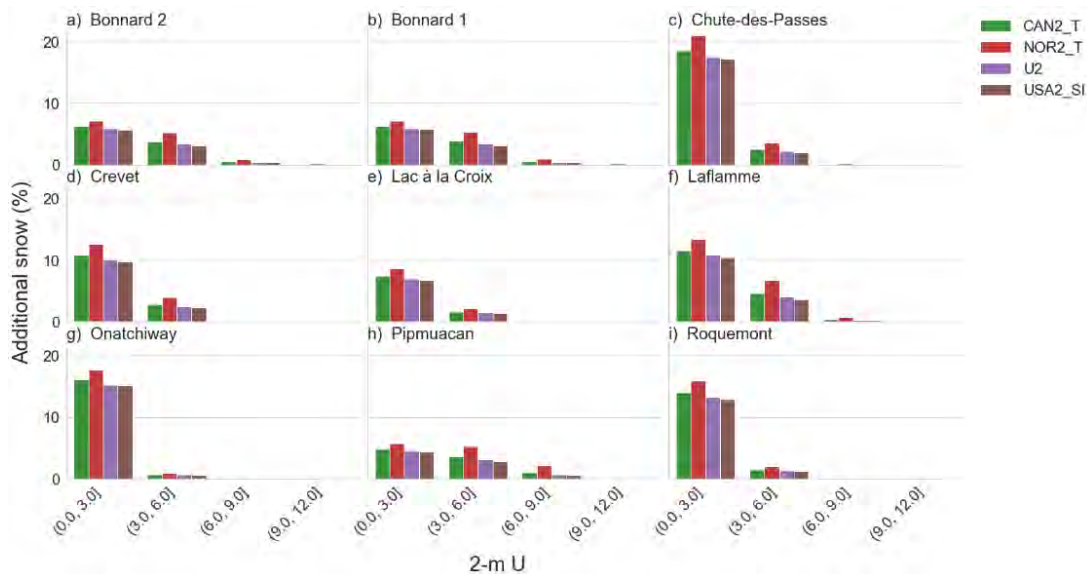


Figure 2.15: The solid cumulated precipitation percentage with the 2-m wind speed (U) effect using the coefficients and equations over the period of 2010 to 2020 for the months of October to April using the $T=-2^{\circ}\text{C}$ partitioning method for available stations.

The selected transfer functions using 10-m wind speed separated by wind speed (U) bins at all sites is presented in Figure 2.16. Three out of the eight sites (Bonnard 1, Bonnard 2 and Pipmuacan) are further corrected to produce more precipitations for wind speeds between 3 to 6 m s⁻¹ than between 0 to 3 m s⁻¹, leading to high corrections at those sites. The corrected precipitation with NOR10 was consistently higher than using UT10.

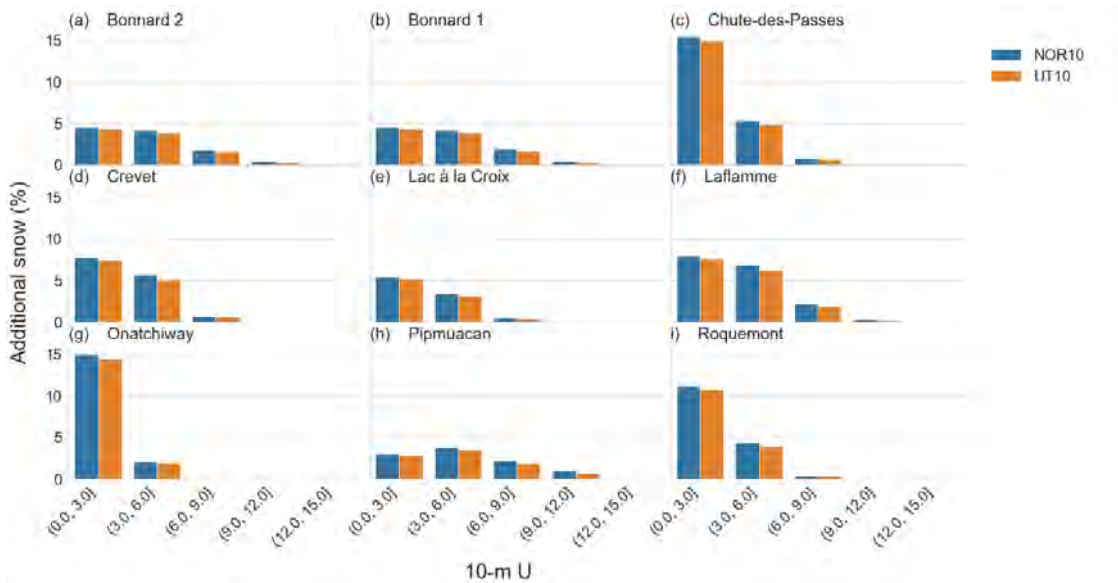


Figure 2.16: Additional corrected solid precipitation amounts relative to measurements (%) with the 10-m wind speed (U) equations for the period of 2010 to 2020 for the months of October to April using the T=-2°C partitioning method.

2.5 Discussion

2.5.1 Phase partitioning methods

A total of four phase partitioning methods were compared at nine meteorological stations over 10 winters. The ratio of solid and liquid precipitation was obtained using a static threshold (T0, T2), a linear threshold (PQ), and a sigmoidal function (Kienzle) allowed to determine the solid fraction of the precipitations every hour. These different phase partitioning methods produced different estimations of annual and monthly solid accumulation (Figure 2.11). These results combined with the annual accumulated number of warm spells per month (Figure 2.9) suggested that the Kienzle method produced the highest solid precipitation fraction during the winters of 2010 and 2015 for all the sites, except for Crevet and Onatchiway since the number of warm spells was higher than at other sites. The year 2015 has the highest proportions of solid precipitation, with an average temperature of -7.7°C (see APPENDIX C for complete average temperature Table). The high percentage of solid precipitation is associated with less warm spells; hence, this shows

that the number of warm spells has a significant impact on the amount of solid precipitation. The winter of 2018 is the period where most of the stations measured the highest solid precipitation amount, with low warm spell counts and an average temperature of -10.0°C being the second-coldest winter. The results between the partitioning methods for the solid portion show a high percentage, but with slightly more variability amongst the methods.

Variability is seen in the relation between the number of warm spells and the annual average temperature (Figure 2.9). For example, the overall highest warm spell counts occurred at Chute-des-Passe station, but has an annual average temperature ranging from -6.0°C to -9.4°C . In contrast, Onatchiway has the warmest annual average with -6.4°C with a relative high spell count, especially during the months of December, January, and February. Therefore, the occurrence of warm spells during the winter months is not necessarily linked to warmer seasonal conditions. Also, wind speed does not have any impact on the solid and liquid ratios.

2.5.2 Range of accumulated snow

In the present study, 16 transfer functions for single-Alter shielded gauge from multiple WMO-SPICE studies were applied to correct the bias of wind undercatch. The corrected accumulated solid precipitation was then compared. Since some results were comparable, with the categorization of similar mean annual bias for the 16 transfer functions allowed us to reduce to six equations (section 2.4.3).

The percentage of accumulated solid precipitation over 10 winters ranged from 8 to 98% more snow per site than what was initially measured at Bersimis-1 and 2 (Figure 2.17). The smallest percentage of additional solid precipitation estimated was obtained by CAN2_T equation with the Kienzle partitioning method and the highest percentage was obtained by NOR2_T with the T2 partitioning method. Even though the highest uncorrected quantities of solid precipitations are obtained with the Kienzle partitioning method, we see the largest adjustments of solid precipitation amount with the T2 method, closely followed by T0. The difference of additional solid precipitation amongst the partitioning methods for the same equation can be explained by the form of each equation, which were obtained using a $T = -2^{\circ}\text{C}$ threshold (Kochendorfer et al., 2017a ; 2017b ; 2018 ; Wolff et al., 2015).

The two equations that produced the largest additional snow are NOR2_T and NOR10, both obtained from the data collected at the WMO-SPICE's Norwegian site. A higher root mean square error was obtained

during the creation of the coefficients at the Norwegian site since the undercatch was large due to strong winds (Kochendorfer 2017a). This means that the effectiveness of the NOR transfer function was lower than the other sites. Hence, this could explain why the NOR equations gave greater adjustments; with a tendency to overcorrect the solid precipitations. However, the type of climate and environment observed at the Norwegian site may be different from the sites on the Bersimis river basin, which could explain why the values are high. This is probably because the Norwegian site is known for its strong winds, where wind speeds above 15 m s^{-1} were measured (Wolff et al., 2015).

The percentage of additional cumulated snow (Equation 2.4, Figure 2.17) is inversely correlated to the number of warm spells and the average temperature as seen for every partitioning method. This could be explained by the fact that most important snowfall events occur at all temperature between 2°C to lower.

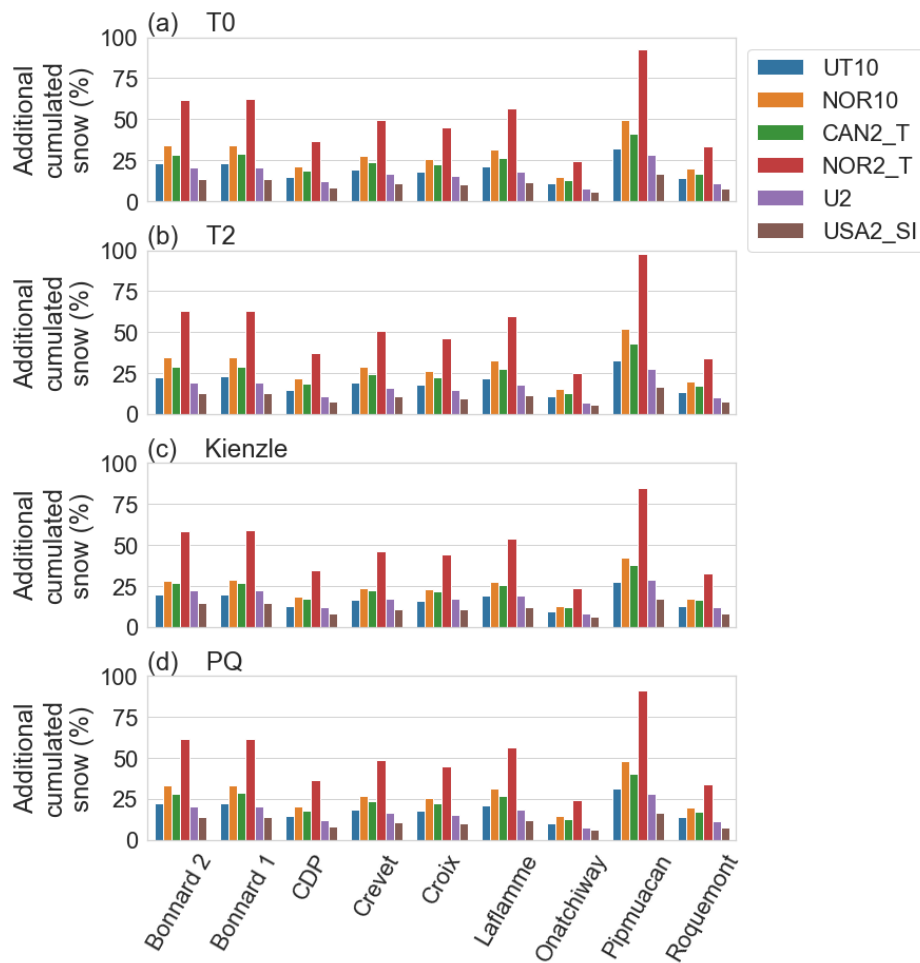


Figure 2.17: The percentage of additional cumulated snow from 2010 to 2020 for the months of October to April for each station for the different phase partitioning methods. a) partitioning method is 0°C or below, b) partitioning

method solid when temperature is -2°C or below, c) Kienzle sigmoidal partitioning method (Kienzle, 2008) and d) Quick and Pipes (1977) partitioning method.

$$\text{Additional cumulated snow (\%)} = \left(\frac{\sum_{i=0}^{n_{\text{event}}} \text{Corrected solid precipitation}_i}{\sum_{i=0}^{n_{\text{event}}} \text{Measured solid precipitation}_i} \times 100 \right) - 100 \quad (2.4)$$

The correlation between the corrected and uncorrected amount of precipitation for the four different partitioning methods, with each panel representing three of the six different transfer functions, are illustrated in Figure 2.18. The six equations are presented in APPENDIX D. Each line representing an equation and column representing a partitioning method, these scatter plots will allow us to understand the weight of each transfer function according to the partitioning method. The mean bias (Mbias, equation 2.5 is also included for each plot. We noticed that the dispersion of the correlation is smallest for USA2_SI for all partitioning methods combined, whereas U2 and NOR10 are more scattered. The Kienzle method illustrates the widest range, and T2 the narrowest. The highest mean bias observed is obtained for NOR2_T with a 0.296 mm h^{-1} (APPENDIX D) with the Kienzle partitioning method. USA2_SI has the smallest dispersion compared to the other equations for the same partitioning methods, which concurs with the results since this equation offered the least amount of additional solid precipitation. U2, the second to last transfer function that offered the least amount of solid precipitation, which also has a low mean bias, has similar range of values compared to UT10 (APPENDIX D) for T0, PQ and T2. The Kienzle partitioning method produced different results. It produced more solid precipitation at higher temperatures than the other partitioning methods. This could mean that U2 is more sensitive to higher temperatures than UT10, but the difference lies in the variable input of the equations, where for U2 uses 2-m wind speed only and UT10 uses temperature and 10-m wind speed.

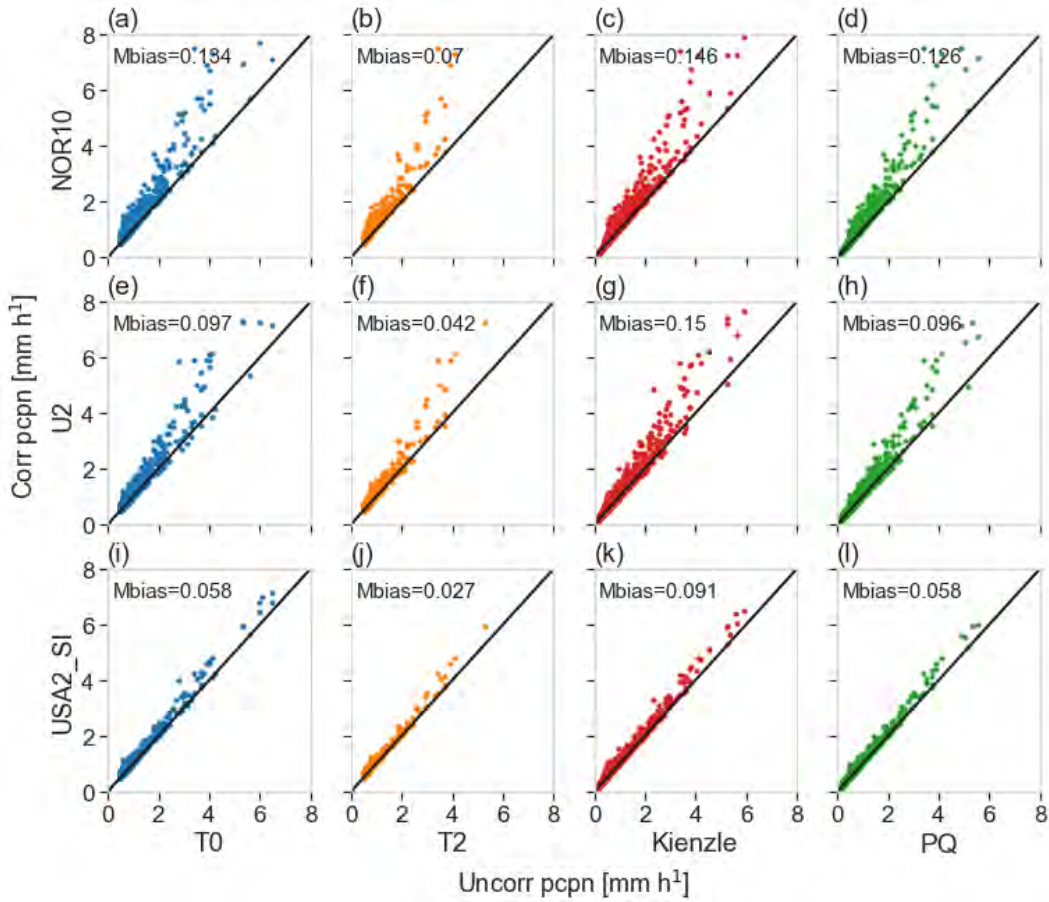


Figure 2.18: Scatter plot of the corrected and uncorrected hourly precipitation [mm] for each partitioning method over the range of temperature between -4°C and $+8^{\circ}\text{C}$. Each line represents a different equation, starting with NOR10, followed by U2 and lastly USA2_SI, described in Table 2. The columns and colours represent the partitioning methods, where blue is the T0 method, orange is T2, red Kienzle and PQ in green. Mbias represents the mean bias between corrected and uncorrected hourly precipitation (Equation 2.5). Data from Chute-des-Passes is illustrated here since it has the highest total precipitation.

$$\text{Mbias} = \text{mean} \left(\frac{\text{Hourly corrected solid precipitation} - \text{Hourly measured solid precipitation}}{\text{Hourly measured solid precipitation}} \right) \quad (2.5)$$

When comparing the results using either the 10-m wind speed input versus the 2-m wind speed input, it is known that using wind corrections at 10-m and gauge height has its strengths and weaknesses. For instance, 10-m wind speed is available at all sites as it is the standard height. The 2-m wind speed is useful because it is the wind speed at near gauge height, which means more representative of the wind speed responsible of the precipitation undercatch. As shown by Kochendorfer et al. (2017a), the CE is strongly correlated to the wind speed measured at gauge height. For this reason, the 2-m wind speed transfer functions are more accurate than the 10-m wind speed when available.

2.5.3 Evaluation of the solid precipitation

The Copernicus Climate Change Service (C3S) at ECMWF produced the ECMWF Reanalysis v5 (ERA5), which provides hourly records of the global atmosphere, land surface and oceanic variables from 1950 onwards (Hersbach et al., 2020). As demonstrated by Betts et al. (2019), the ERA5 precipitation during winter in the Canadian Prairies are slightly overestimated, but overall, the precipitation and water budgets seem realistic.

The uncorrected solid precipitation amounts are compared with ERA5 over the Bersimis river basin (Figure 2.19). We notice a large variability between the stations and phase partitioning methods (Figure 2.19). First, the total solid precipitation from ERA5 is below the measured at Chute-des-Passes (CDP), Lac à la Croix (Croix), Pipmuacan, Roquemont and Onatchiway for all partitioning methods. Second, the Kienzle method consistently gives higher values than the ones from ERA5. For Crevet, the uncorrected precipitation using T0 and PQ method are similar to ERA5. The precipitation measured at Laflamme is higher for every method except T2 and for both Crevet and Laflamme, T2 method was lower. Finally, for Bonnard 1 and 2, T0, T2 and PQ show that the uncorrected solid precipitation amount is less than ERA5.

Depending on the partitioning method, the uncorrected solid precipitations are close to ERA5, whereas the Kienzle method obtained the highest solid precipitation amounts (Figure 2.19). For the other partitioning methods at Bonnard 1 and Bonnard 2, the measured uncorrected solid precipitation is lower than ERA5. In contrast, at the same locations for T0 and PQ partitioning methods, USA2_SI is closest to ERA5. For T2 method, NOR10 is like ERA5. As for the other sites, the precipitation amounts were all higher compared to ERA5.

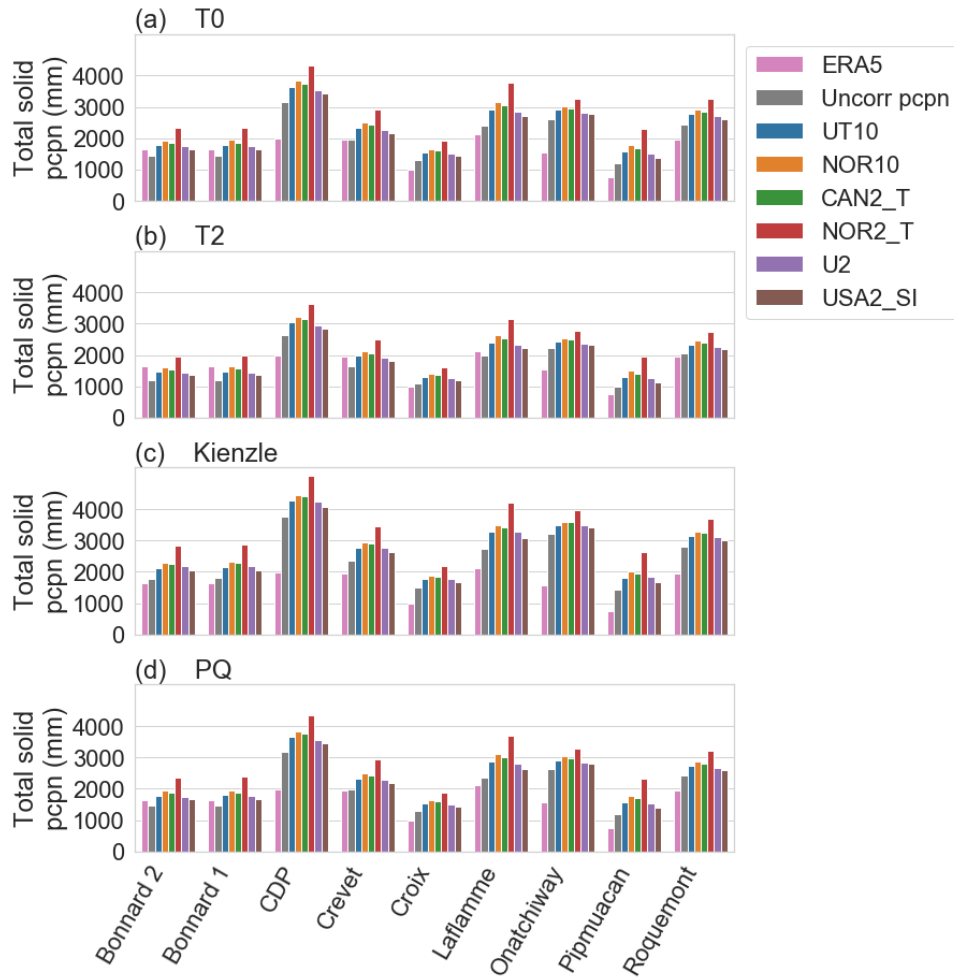


Figure 2.19: Total cumulated measured and corrected solid precipitation from 2010 to 2020 for the months of October to April for each station compared to ERA5 reanalysis data (pink). a) partitioning method is 0°C, b) partitioning method solid when temperature is -2°C or below, c) Kienzle sigmoidal partitioning method and d) Quick and Pipes (1977) partitioning method.

The annual mean uncorrected and corrected solid precipitation amounts are compared with ERA5 (Figure 2.20). At Crevet, Bonnard 1 and Bonnard 2, the ERA5 mean is less than the uncorrected precipitation for T0, T2 and PQ. The UT10, NOR10, CAN2_T, U2 and USA2_SI are often like ERA5 for these three stations. For all sites and partitioning methods, NOR2_T overcorrects solid precipitation the most compared the other transfer functions and ERA5.

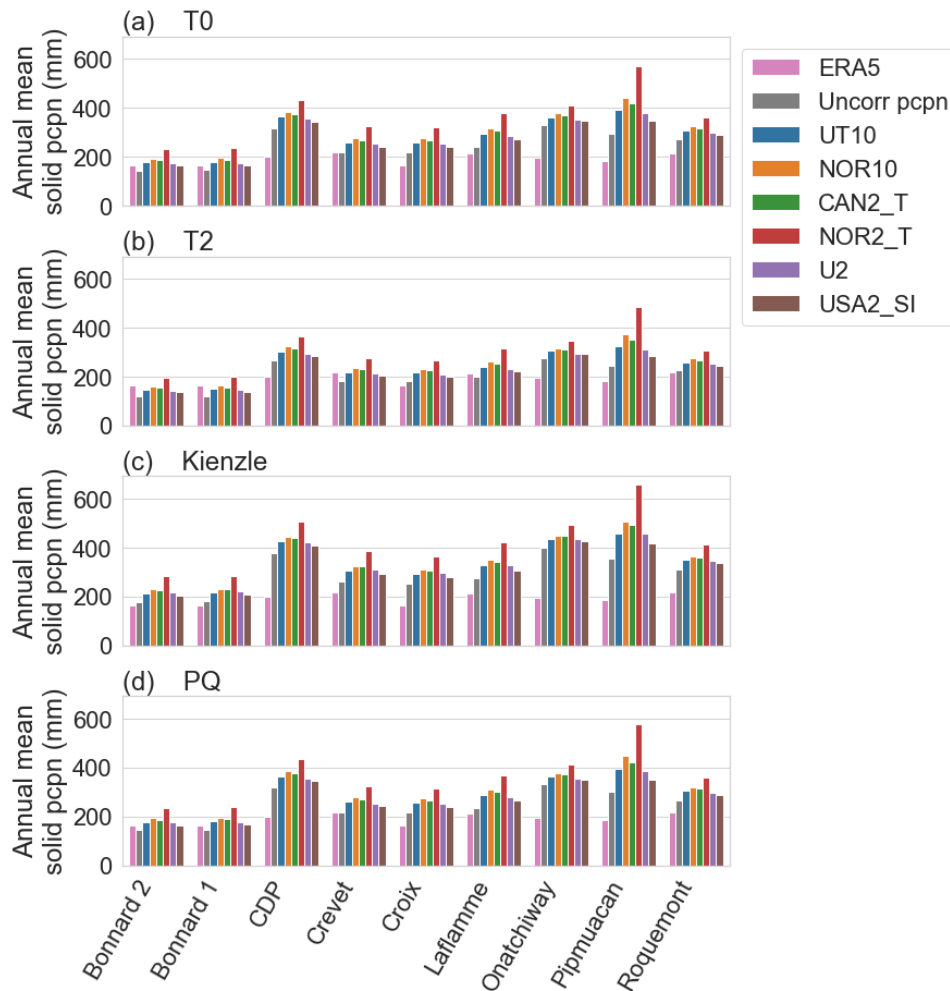


Figure 2.20: Annual cumulated mean solid precipitation for measured and corrected solid precipitation from 2010 to 2020 for the months of October to April for each station compared to ERA5 reanalysis data (pink). a) partitioning method is 0°C, b) partitioning method solid when temperature is -2°C or below, c) Kienzle sigmoidal partitioning method and d) Quick and Pipes (1977) partitioning method.

The mean annual solid precipitation bias between the corrected and the uncorrected solid precipitation amounts with respect to ERA are shown Figure 2.21. The mean annual bias is obtained by adding up the winter years total solid precipitation amounts and subtracting it to its corresponding sum proposed by ERA5. After obtaining a yearly difference for each equation and partitioning method combination, we calculate the mean over the 10 years. The differences are greater for Chute-des-Passes (CDP), Onatchiway and Pipmuacan. For Crevet, Bonnard 1 and Bonnard 2, the annual differences are lowest. The Kienzle method and the NOR2_T propose the largest differences with ERA5. For all stations, the T2 partitioning method is closest to ERA5, with the smallest bias amongst all the other partitioning methods. For Bonnard 1 and Bonnard 2, NOR10 is closest to ERA5's solid mean annual solid precipitation amount, with the T2

partitioning method. For Crevet, UT10 with T2 best represent the precipitations compared to ERA5. For the remaining sites, the bias ranges between 50 to 250 mm over ERA5's mean annual solid precipitation.

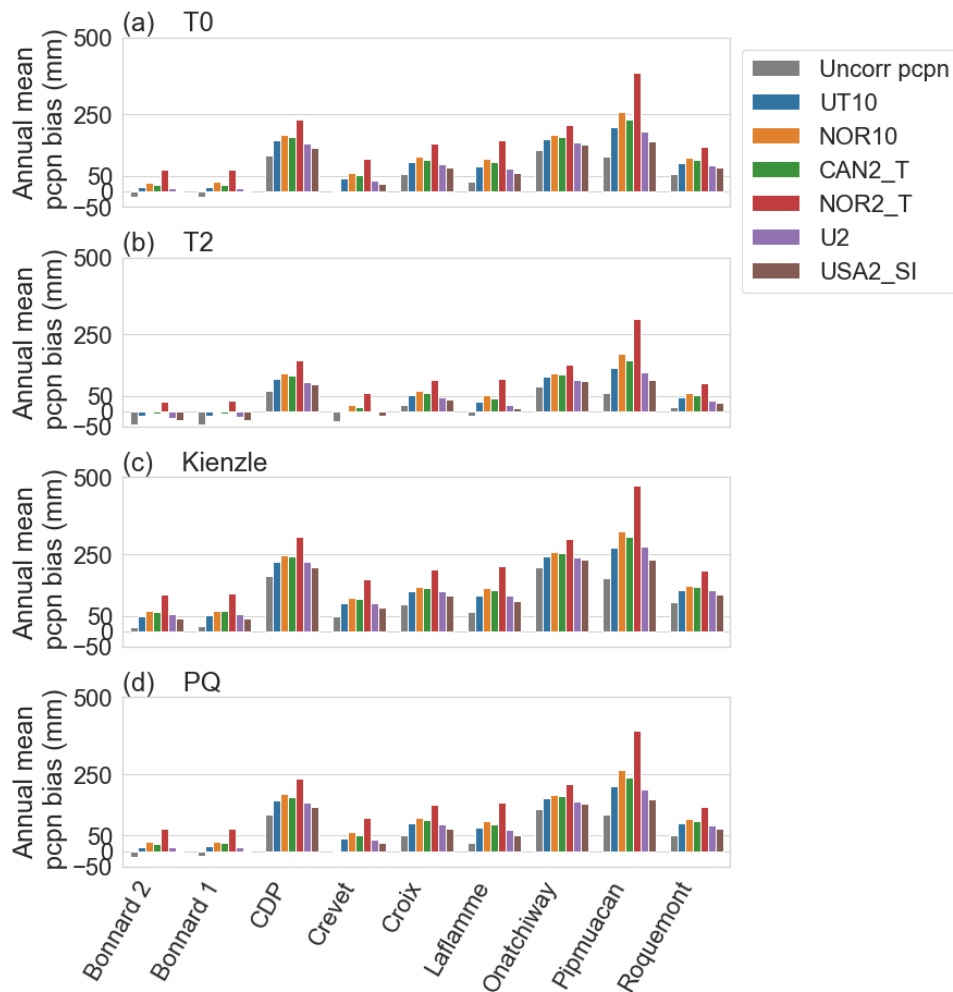


Figure 2.21: Mean annual bias per station of ERA5's solid precipitation estimation compared to the corrections and uncorrected solid precipitation data for the six transfer functions illustrated by partitioning method for a) temperature threshold is 0°C, b) temperature threshold is -2°C or below, c) Kienzle sigmoidal transition and d) Quick and Pipes (1977) linear transition.

The ERA5 data is lower compared to the measured amounts at most of the sites. Compared to site measurements, the ERA5 reanalysis uses historic observations such as satellite, *in-situ* measurements, radiosonde, snow depth data and more (Hersbach et al., 2020). Xiong et al. (2022) compared ERA5 with the Integrated Multi Satellite Retrievals for Global Precipitation Measurement (IMERG) and found good agreement in the arctic region. They stated that the same conclusions do not apply to mid- and low-latitude regions, meaning that solid precipitation amounts from ERA5 could be misleading. An interesting

possibility would be to compare the results with different reanalysis or observational products such as the Canadian Precipitation Analysis (CaPA).

2.5.4 Implication on hydrology

Estimating the accurate precipitation amount and phase is crucial for hydrological prediction. A key input in hydrology is the snow depth (snow on the ground), which strongly relies on precipitation measurement (Brown et al., 2018). Either the precipitation will run off into the ground, melt in the snow cover or flow into rivers if it falls as liquid, or either it will fall as solid precipitation and accumulate on ground. As shown in this recent study evaluating the snow water equivalent for a Hydro-Quebec River basin (Brown et al., 2018), the lack of solid precipitation accuracy, due to wind undercatchment, impacts the short- and long-term hydrological forecasts resulting in a failure to respect Hydro-Quebec's operational requirements.

We showed that phase partitioning methods and different transfer functions can result in large differences in the estimated accumulated snowfall. These variations in snowfall with the different methods should be accounted for in hydrological model as the precipitation phase is often measured to understand the hydrological response to the different combinations of partitioning and undercatchment transfer functions. Further studies should consider comparing different phase partitioning methods with disdrometer measurements, as done in Casellas et al. (2021) in Spain. Knowing the type of precipitation when it reaches the ground will allow us to better understand its behaviour subsequently and automate the phase partitioning. In addition, the other processes influencing the snowpack on the ground such the precipitation type will help predict how the hydrological cycle will react (Harpold et al., 2017). The amount of precipitation corrected by the wind undercatch will directly impact the hydrological cycle, and probably increase the measured amount of water available in spring during the snowmelt season.

2.6 Summary and Conclusions

2.6.1 Summary

In this study, the solid precipitation wind undercatch was investigated over the Bersimis river basin. Data from nine Hydro Quebec meteorological stations over the Bersimis river basin, Quebec, Canada, were used. Four partitioning methods were used to determine the liquid fraction. Solid precipitation was only adjusted on the amount diagnosed by those phase partitioning methods. Solid precipitation amounts were adjusted for wind speed undercatch using transfer functions developed by WMO-SPICE experiments (Goodison et

al., 1998 ; Kochendorfer et al., 2017a ; 2017b ; 2018 ; Colli et al., 2020). A total of six transfer functions were selected as they produced a range of precipitation amounts.

The range of snow accumulation using the combination of phase partitioning and transfer functions were then compared amongst them and against ERA5 reanalysis. Overall, the Kienzle partitioning method (sigmoidal function) resulted in the highest quantities of solid precipitation, whereas the T2 partitioning method (constant threshold for solid precipitation set to -2°C) obtained the lowest amount of solid precipitation. Regarding the transfer functions, amongst the six compared equations, the NOR equations were proven to propose the largest corrections since the site where the coefficients were created has strong wind conditions. The transfer function that proposed the smallest corrections was USA2_SI, a transfer function using 2-m wind speed and snowfall intensity (mm h^{-1}) with coefficients computed from the US testing site. Even though the Kienzle method offered more solid precipitation than the other methods, the largest corrections were observed with the T2 method since the transfer functions were created using this threshold (Equations 2.1 & 2.2 ; Kochendorfer et al., 2017a ; 2017b). We noticed that the ERA5 precipitations are below the initial uncorrected solid precipitation amounts.

This study focuses on the range of solid precipitation accumulation using four phase partitioning methods to diagnose the amount of snow measured and then added percentage from the transfer functions to adjust the total amount of snow for wind undercatch. The combination of three studies on estimating the undercatch and four precipitation fractioning methods were applied on 10 winters of nine different sites. The objective of this study was to evaluate the potential of snowfall deviated by wind at the entrance of a Single Alter shielded automatic gauge with the use of either wind speed only, air temperature combined to wind speed and snowfall intensity with wind speed.

2.6.2 Conclusions

The results obtained allowed us to study the different behaviours of the multiple transfer functions proposed by Kochendorfer and Colli (Kochendorfer et al., 2017a ; 2017b ; Colli et al., 2020). The analysis led to the following conclusions:

- The snow water equivalent ranges from around 2,500 to 5,000 mm per year over the Bersimis river basin. For wind speed, the 10-m wind speed was often below 5 m s^{-1} , but Laflamme, Bonnard 1 and Bonnard 2 were the fastest winds recorded and detected 10-m wind speed as high as 10 m s^{-1} . During

this period, the mean 2-m air temperature could reach as low as -40°C and up to over 20°C . For six out of the nine sites, the most common temperature observed was between -2°C and 2°C . Even though those temperatures were reached mostly during the shoulder months of the winter season, some thaws were recorded all winter long. Onatchiway recorded the highest count of warm spells from December to March. When looking at the annual distribution of accumulated warm spells, Onatchiway reached more than 1,000 occurrences of warm spells, followed by Chute-des-Passes.

- A total of four phase partitioning methods were applied to the total hourly precipitation data to obtain solid and liquid precipitation amounts. Two methods used a static air temperature threshold; 0°C and -2°C , another one proposed a linear transition (PQ) from -2°C to 2°C and finally a last method suggested a sigmoidal transition (Kienzle) from -4°C to 8°C . When comparing the different partitioning methods amongst themselves, we noticed that the Kienzle partitioning method gave the most solid precipitations and the -2°C (T2) gave the least. T0 and PQ performed similarly, obtaining mid-ranged amounts between the Kienzle and T2 methods. The total solid precipitation ranged between 30% to 80% each year for T0 and PQ.
- Once the solid part of the precipitation was identified, the application of the 16 transfer functions was realized. Since the corrections from the multiple transfer functions were redundant, six different equations were selected: UT10, NOR10, CAN2_T, NOR2_T, U2 and USA2_SI. The equations from Norway (NOR) proposed the highest corrections whereas USA2_SI proposed the smallest. The corrections were evaluated according to the wind speed, temperature and snowfall intensity used. The mean correction for most of the sites ranged from an addition of 15 to 100 mm of solid precipitations per year. The station that measured the most precipitations using the Norwegian equation obtained a correction of 239 mm more solid precipitation during winter. Even though most of the precipitations occurred at low wind speeds, corrections between 3 to 6 m s^{-1} offer higher corrections than at lower wind speeds for the same precipitation measured initially. The stronger the winds, the more precipitation is blown away from the precipitation gauge, meaning that the transfer function corrects more when needed. The results obtained from the four partitioning methods and the six transfer functions gave a total of 24 solid wind-bias corrections. Even though the Kienzle method offered the most solid precipitations, the added percentage corrected from the equations was obtained using the T2 method.
- ERA5 is often below the uncorrected solid precipitation for all partitioning methods at all sites, except for Bonnard 1 and Bonnard 2 when using the T0, T2 and PQ partitioning methods. As for the corrections

proposed by the transfer functions compared to ERA5, the corrections were above the ERA5 values. Therefore, a lot of variability was found between the adjusted precipitation and ERA5.

This study has few limitations. First, errors in the data filtering could be reduced using real-time review of the data to improve the data quality. Second, applying phase partitioning methods that include the effect of humidity could improve the results. Casellas et al. (2021) and Harder and Pomeroy (2013) showed that using a constant wet bulb temperature or dew point temperature threshold provided the best estimates of solid vs liquid precipitation. Third, choosing meteorological sites that have more equipment available to compare the precipitation results such as a Gamma MONitor (GMON) to obtain the snow water equivalent (SWE) could help validate the results. This instrument measures the absorption of the natural gamma radiation through the snow cover (Choquette et al., 2008). A disdrometer or a camera to detect the precipitation phase could also be useful for the validation of the phase partitioning. Fourthly, future work to understand which equation would be the best fit for the climate observed at Bersimis river basin would be interesting. Then, the best transfer function could be applied at each site for the entire Hydro-Quebec territory to provide better initial conditions for the hydrological model.

Finally, this study allowed to better understand the range of measurements of precipitation accumulating during the cold season over the Bersimis River Basin, Quebec, Canada. The high variability of the precipitation amounts based on the phase partitioning method and transfer function highlight the challenge in accurately measuring snowfall. Nevertheless, this information can be used to better estimate the accurate precipitation amounts and, in turn, improve the hydrological predictions for hydroelectricity production at Hydro-Quebec.

CHAPITRE 3 CONCLUSION

Dans cette étude, les difficultés liées à la mesure des précipitations hivernales ont été abordées. De nombreuses erreurs persistent lors de la quantification des précipitations avec une jauge automatique. Ces erreurs de mesure impactent diverses sphères, dont la météorologie et l'hydrologie. En effet, la modélisation météorologique et hydrologique nécessite des données de précipitations justes, surtout au Québec où la source principale d'électricité provient de certains bassins versants sur le territoire (Hydro-Québec B, 1996-2022). Le but de cette étude était de diminuer les erreurs liées à la sous-captation des précipitations solides causée par le vent. Grâce au réseau météorologique d'Hydro-Québec, les données de neuf sites sur le bassin de la rivière Bersimis, Québec, Canada, ont pu être utilisées pour appliquer des méthodes issues de la littérature dans le but de réduire le biais dû à la sous-captation par le vent. À cette fin, la détermination de la fraction solide et liquide était nécessaire. Quatre méthodes différentes, dont une fonction sigmoïdale, ont été utilisées dans cette étude. Une fois la fraction solide déterminée, les fonctions de transfert des expériences de l'OMM sur l'étude des précipitations solides (SPICE) ont été appliquées (Goodison et al., 1998 ; Kochendorfer et al., 2017a ; 2017b ; 2018 ; Colli et al., 2020). Un total de 16 fonctions de transfert a été analysé, dont six qui ont été sélectionnées en raison de comportements répétitifs parmi les autres équations. La valeur ajoutée de la combinaison de la séparation des phases solides et liquides, avec la correction due à la sous-captation par le vent pour la partie solide, a pu être analysée et comparée entre elles. Les différentes combinaisons de résultats ont également été comparées avec les précipitations solides estimées par les produits de réanalyse d'ERA5.

Tout d'abord, les données horaires récoltées par les neuf stations météorologiques ont subi un contrôle de qualité et un filtrage des données afin de supprimer le bruit et les mesures aberrantes présents dans les données brutes. Par la suite, une analyse des conditions climatiques a démontré que les conditions de vitesse du vent dans ce climat varient autour de 0 à 5 m s⁻¹ pour certains sites, mais peuvent aller jusqu'à 10 m s⁻¹ lorsque l'on mesure des vitesses de vent à 10 m, justifiant le besoin de corriger les effets de la sous-captation due au vent. Une analyse de la climatologie de la température a été également nécessaire afin de dresser un portrait de la fluctuation de la forme des précipitations. Il en est ressorti que la température moyenne de l'air, mesurée à 2 m, varie de telle sorte que celle-ci peut descendre jusqu'à -40°C ou encore dépasser les 0°C durant les mois d'octobre à avril. De plus, pour six des neuf sites, la température la plus couramment observée se situait entre -2°C et 2°C ; les températures où l'on peut observer des changements de phase dans les précipitations (Stewart et al., 2015 ; Harder and Pomeroy,

2013). Même si ces températures ont été atteintes principalement durant les mois d'octobre et avril, des dégels ont tout de même eu lieu tout au long de l'hiver. Parmi tous les sites, Onatchiway est la station qui a enregistré la plus grande quantité de redoux de décembre à mars.

Une fois les données météorologiques analysées, l'analyse des méthodes de séparation pluie-neige a été effectuée. Un total de quatre différentes méthodes de séparation a été testé afin d'obtenir les précipitations solides et liquides à partir des précipitations totales. Deux méthodes utilisent un seuil de température de l'air statique de 0°C (T0) et -2°C (T2), la troisième méthode de partition est composée d'une transition linéaire (PQ) de -2°C à 2°C et enfin la dernière méthode applique une transition sigmoïdale de -4°C à 8°C (Kienzle). Les résultats ont montré que le partitionnement de Kienzle est celui qui génère les plus grandes quantités de précipitations solides parmi les quatre. La méthode de séparation des phases utilisant le seuil de précipitation solide fixé à -2°C est celle qui offre le moins de précipitations solides.

Une fois la partie solide de la précipitation identifiée, l'application des 16 fonctions de transfert a été réalisée. Comme les corrections des fonctions de transfert multiples étaient semblables, six équations différentes ont été sélectionnées : UT10, NOR10, CAN2_T, NOR2_T, U2 et USA2_SI. Parmi les six équations, les équations de la Norvège (NOR2_T et NOR10) proposaient en moyenne des corrections trois fois plus grandes que l'équation qui offrait la plus petite correction, soit USA2_SI. La première utilisant la vitesse de vent à 2 m ainsi que la température de l'air et la seconde la vitesse de vent mesurée à 10 m ainsi que la température de l'air. Ceci s'explique par l'emplacement du site où les coefficients ont été créés, c'est-à-dire dans des conditions de vent fort (Wolff et al., 2015). La fonction de transfert qui proposait les plus petites corrections est USA2_SI, une fonction de transfert utilisant la vitesse du vent à 2 m et l'intensité des chutes de neige (mm h^{-1}) avec des coefficients calculés à partir du site des États-Unis. En effet, pour la plupart des sites, une correction moyenne était possible de varier de 15 à 100 mm de précipitations solides par an selon l'équation et la méthode de séparation de phase choisie. Les corrections ont été évaluées en fonction de la vitesse du vent utilisée. Bien que la plupart des précipitations sont produites à des vitesses de vent relativement faibles, les corrections les plus importantes par quantité de précipitations solides se situent entre 3 et 6 m s^{-1} ou plus. Plus les vents sont forts, plus les précipitations sont déviées de l'entrée de la jauge automatique (Thériault et al., 2012). Ceci signifie que les fonctions de transfert corrigent davantage lorsque la déviation est la plus importante. Somme toute, les résultats obtenus à partir des quatre méthodes de partition de la phase et des six fonctions de transfert ont donné un total de 24 combinaisons de corrections solides pour la sous-captation due au vent. La comparaison entre les

méthodes a permis de montrer que même si la méthode de séparation pluie-neige de Kienzle offrait plus de précipitation solide que les autres méthodes, les corrections les plus importantes sont observées avec la méthode T2. Ceci s'explique par le fait que les fonctions de transfert ont été créées à partir de ce seuil (Kochendorfer et al., 2017a ; 2017b).

Afin d'analyser le tout, les données d'Hydro-Québec ont été comparées à celles de la réanalyse d'ERA5. Une conclusion provenant de cette comparaison est que les quantités initiales de précipitations solides non corrigées sont souvent supérieures à celles d'ERA5. En effet, Xiong et al. (2022) ont montré que l'efficacité du produit de réanalyse ERA5 aux latitudes moyennes pour les précipitations solides ne représentait pas aussi bien les conditions réelles comparativement en Arctique. Ceci fait en sorte qu'une grande variabilité est observée entre les résultats des différentes combinaisons de partition de la phase ainsi que de correction de sous-captation avec le produit de réanalyse d'ERA5.

Les avantages reliés à l'utilisation d'équations de transfert sur des données de précipitations en quasi-temps réel pour l'ensemble du territoire d'Hydro-Québec permettraient d'offrir de meilleures conditions initiales en équivalence en eau de la neige au modèle hydrologique. À ce jour, Hydro-Québec a mis en place la possibilité d'estimer les valeurs corrigées pour des précipitations solides à des fins expérimentales. Il est prévu de rendre ce processus opérationnel afin d'améliorer les prévisions hydrologiques à l'échelle de bassin versant. De plus, d'autres alternatives de séparation des phases pourraient être ajoutées à la suite de cette étude, certaines tenant compte de l'effet de l'humidité dans les méthodes de séparation des phases. Casellas et al. (2021) et Harder et Pomeroy (2013) ont montré que l'utilisation d'un seuil de température de bulbe humide ou de point de rosée constant fournissait les meilleures estimations des précipitations solides par rapport aux précipitations liquides.

Dans l'ensemble, cette étude s'est concentré la correction de biais dû à la sous-captation et au partitionnement des précipitations solides. Pour ce faire, quatre méthodes de fractionnement des précipitations ainsi que des six équations sur l'estimation de la sous-captation par le vent ont été appliquées sur 10 hivers, et ce, sur neuf sites différents. Ceci a permis d'obtenir un éventail de précipitations solides corrigées. Ces corrections de précipitations ont pu être réalisées à partir des variables qui impactent la sous-captation et le changement de phase, c'est-à-dire la vitesse du vent, la température de l'air et le taux de précipitation. C'est à partir de plusieurs fonctions de transfert proposées par Kochendorfer et Colli (Kochendorfer et al., 2017a ; 2017b ; Colli et al., 2020) qu'une évaluation des

différentes corrections de précipitations solides a été réalisée. Les résultats présentés dans ce mémoire ont permis d'appliquer directement la méthodologie d'études antérieures sur la sous-captation et le partitionnement de phases. Dans le but d'obtenir un éventail de précipitations corrigées utilisables comme intrant d'équivalence en eau de la neige dans les prévisions hydrologiques à Hydro-Québec.

APPENDIX A
Station Lac à la Croix

Vue aérienne d'une station permettant d'observer le type de végétation, le degré de déboisement ainsi que la configuration des instruments de mesure



Figure A. 1: Exemple d'une station météorologique typique avec hélicoptère. Photo d'Hydro-Québec Production.

APPENDIX B

Méthodes de séparation pluie-neige

Le modèle canadien UBC Watershed (Quick and Pipes, 1977) utilise une méthode de transition de phase linéaire. Cette méthode de partition offre un changement graduel entre les fractions liquides et solides. Puisque l'on peut retrouver des précipitations solides, mixtes ou liquides à des températures de l'air entre 2°C et -2°C, ces températures respectives ont été choisies comme seuils pour différencier le liquide du solide.

Pour PQ:

$P_{\text{rain}} = 1$, lorsque $T \geq 2$ (100% liquide)

$P_{\text{rain}} = T/4 + 0.5$, lorsque $T < 2$ and $T \geq -2$

$P_{\text{rain}} = 0$, lorsque $T \leq -2$ (100% solide):

où P_{rain} est la fraction liquide. La fraction solide est obtenue comme suit : $P_{\text{snow}} = P_{\text{rain}} - 1$.

Une étude plus récente pour déterminer le type de phase est par l'utilisation d'une fonction sigmoïdale de la température (Kienzle, 2008). La température moyenne journalière est exprimée par T_T et le « range » de température (T_R) représente la fenêtre où l'on peut retrouver des précipitations solides, liquides ou mixtes selon Kienzle (2008). Puisqu'aucune observation du type de précipitations n'a été réalisés durant cette étude, les valeurs moyennes proposées par l'auteur ont été utilisées, c'est-à-dire $T_T = 2.6^\circ\text{C}$ et $T_R = 13.3^\circ\text{C}$.

Pour $T \leq T_T$ et $P_{\text{rain}} \geq 0$:
$$P_{\text{rain}} = 5 \times \left(\frac{T-T_T}{1.4 \times T_R} \right)^3 + 6.76 \times \left(\frac{T-T_T}{1.4 \times T_R} \right)^2 + 3.19 \times \left(\frac{T-T_T}{1.4 \times T_R} \right) + 0.5$$

Pour $T \geq T_T$ et $P_{\text{rain}} \leq 1$:
$$P_{\text{rain}} = 5 \times \left(\frac{T-T_T}{1.4 \times T_R} \right)^3 - 6.76 \times \left(\frac{T-T_T}{1.4 \times T_R} \right)^2 + 3.19 \times \left(\frac{T-T_T}{1.4 \times T_R} \right) + 0.5$$

APPENDIX C

Températures moyennes annuelles

	2010	2011	2012	2013	2014	2015
Bonnard 2	-8.8	-8.0	-7.7	-11.0	-11.8	-8.8
Bonnard 1	-8.8	-8.0	-7.7	-11.0	-11.9	-8.8
Chute-des-Passes	-6.7	-6.0	-6.2	-9.3	-9.7	-6.9
Crevet	-6.4	-5.9	-5.2	-5.1	-9.1	-6.9
Lac à la Croix	-7.4	-8.6	-7.1	-9.8	-12.0	-9.5
Laflamme	-6.9	-5.3	-6.3	-8.1	-9.5	-6.7
Onatchiway	-6.1	-4.4	-6.0	-8.1	-8.2	-5.3
Pipmuacan	-7.0	-5.9	-6.1	-9.3	-9.3	-7.0
Roquemont	-8.4	-8.5	-1.6	0.3	-11.7	-9.4
Moyenne annuelle	-7.4	-6.7	-6.0	-7.9	-10.4	-7.7

	2016	2017	2018	2019	Moyenne aux stations
Bonnard 2	-8.5	-9.7	-11.0	-9.2	-9.5
Bonnard 1	-8.5	-9.7	-11.0	-9.3	-9.5
Chute-des-Passes	-6.6	-7.8	-9.4	-7.7	-7.6
Crevet	-6.5	-7.6	-9.2	-7.2	-6.9
Lac à la Croix	-9.0	-10.0	-11.2	-9.4	-9.4
Laflamme	-6.6	-7.6	-9.8	-7.1	-7.4
Onatchiway	-5.3	-6.4	-8.0	-6.4	-6.4
Pipmuacan	-4.5	-7.6	-9.5	-7.2	-7.3
Roquemont	-8.8	-9.8	-11.3	-9.3	-7.9
Moyenne annuelle	-7.1	-8.5	-10.0	-8.1	-8.0

Table C. 1 : Détail des températures moyennes annuelles par site pour chaque année respective.

APPENDIX D

Résultats entiers des nuages de points de la Figure 2.18.

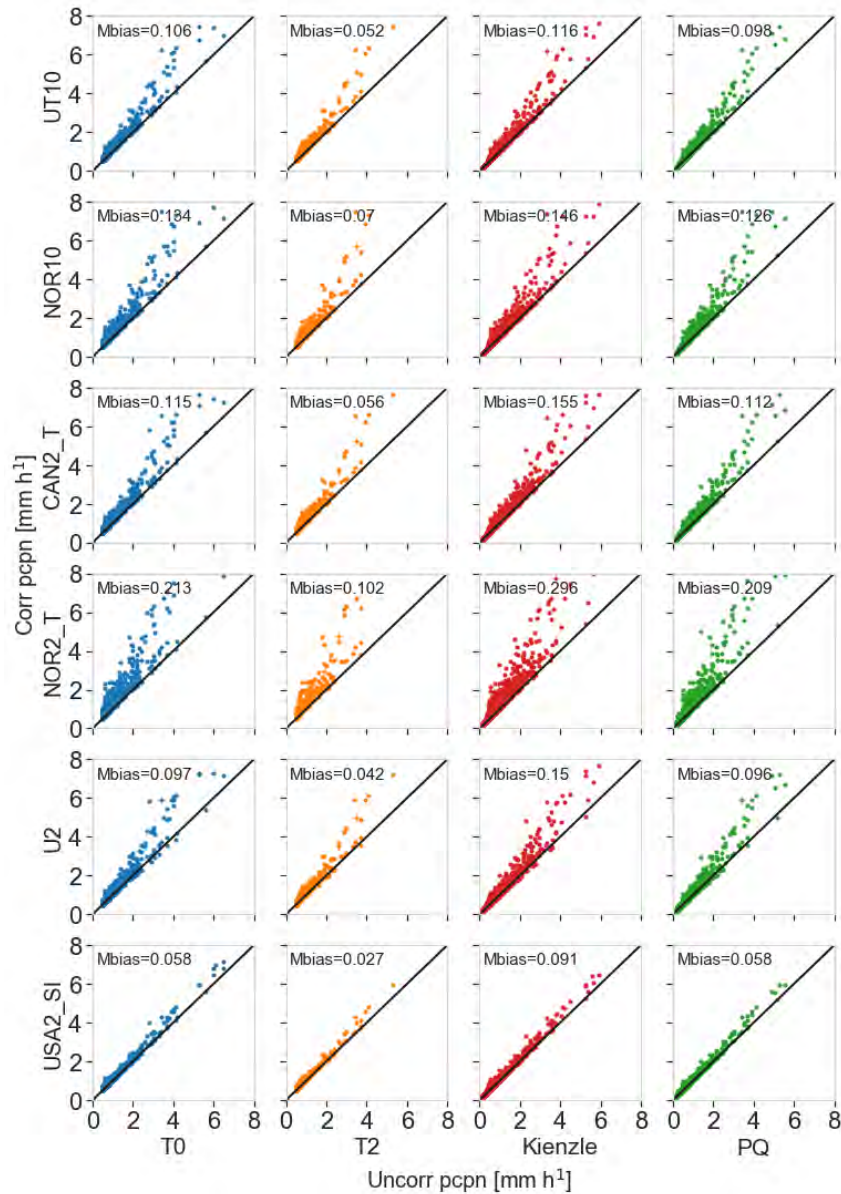


Figure D. 1: Nuage de points des précipitations horaires corrigées et non corrigées [mm] pour chaque méthode de partition de température entre -4°C et +8°C. Chaque ligne représente une équation différente, en commençant par UT10, NOR10, CAN2_T, NOR2_T, U2 et USA2_SI, détaillées à la Table 2.2. Les colonnes et les couleurs représentent les méthodes de partitionnement, où le bleu est la méthode T0, l'orange est T2, le rouge Kienzle et PQ le vert. Mbias représente le biais moyen entre les précipitations horaires corrigées et non corrigées. Les données de Chute-des-Passes sont illustrées ici puisqu'elles ont les précipitations totales les plus élevées.

RÉFÉRENCES

- Alter, J. C. (1937). Shielded storage precipitation gauges. *Monthly Weather Review*, 65(7), 262-265.
- Auer, A. H. (1974). The rain versus snow threshold temperatures, *Weatherwise*, 27, 67.
- Betts, A. K., Chan, D. Z., & Desjardins, R. L. (2019). Near-surface biases in ERA5 over the Canadian prairies. *Frontiers in Environmental Science*, 7, 129.
- Brown, R., Tapsoba, D., & Derksen, C. (2018). Evaluation of snow water equivalent datasets over the Saint-Maurice River basin region of southern Quebec. *Hydrological Processes*, 32(17), 2748-2764.
- Buisán, S. T., Earle, M. E., Collado, J. L., Kochendorfer, J., Alastrué, J., Wolff, M., ... & López-Moreno, J. I. (2017). Assessment of snowfall accumulation underestimation by tipping bucket gauges in the Spanish operational network. *Atmospheric Measurement Techniques*, 10(3), 1079-1091.
- Casellas, E., Bech, J., Veciana, R., Pineda, N., Rigo, T., Miró, J. R., & Sairouni, A. (2021). Surface precipitation phase discrimination in complex terrain. *Journal of Hydrology*, 592, 125780.
- Choquette, Y., Lavigne, P., Nadeau, M., Ducharme, P., Martin, J. P., Houdayer, A., & Rogoza, J. (2008, September). GMON, a new sensor for snow water equivalent via gamma monitoring. In *Proceedings Whistler 2008 International Snow Science Workshop September 21-27, 2008* (p. 802).
- Cloke, H. L., & Pappenberger, F. (2009). Ensemble flood forecasting: A review. *Journal of hydrology*, 375(3-4), 613-626.
- Colli, M., Rasmussen, R., Thériault, J. M., Lanza, L. G., Baker, C. B., & Kochendorfer, J. (2015). An improved trajectory model to evaluate the collection performance of snow gauges. *Journal of Applied Meteorology and Climatology*, 54(8), 1826-1836.
- Colli, M., Lanza, L., Rasmussen, R., & Thériault, J. (2016, April). Advances in the evaluation of wind-induced undercatch using CFD-based simulations of snow gauge performance. In *EGU General Assembly Conference Abstracts* (pp. EPSC2016-10822).
- Colli, M., Stagnaro, M., Lanza, L. G., Rasmussen, R., & Thériault, J. M. (2020). Adjustments for wind-induced undercatch in snowfall measurements based on precipitation intensity. *Journal of Hydrometeorology*, 21(5), 1039-1050.
- Dai, A. (2008). Temperature and pressure dependence of the rain-snow phase transition over land and ocean. *Geophysical Research Letters*, 35(12).
- Devia, G. K., Ganasri, B. P., & Dwarakish, G. S. (2015). A review on hydrological models. *Aquatic procedia*, 4, 1001-1007.
- Førland, E. J., Allerup, P., Dahlström, B., Elomaa, E., Jónsson, T., Madsen, H., ... & Vejen, F. (1996). Manual for operational correction of Nordic precipitation data. *DNMI-Reports*, 24(96), 66.

- Glickman, T. S. (2000). *Glossary of Meteorology*, Am. Meteorol. Soc., Boston, Mass.
- Golubev, V. S. (1989). Assessment of accuracy characteristics of the reference precipitation gauge with a double-fence shelter. *Final report of the Fourth Session of the International Organizing Committee for the WMO solid precipitation measurement intercomparison*, 22, 29.
- Goodison, B. E. (1978). Accuracy of Canadian snow gage measurements. *Journal of Applied Meteorology and Climatology*, 17(10), 1542-1548.
- Goodison, B., & Yang, D. (1996). In situ measurements of solid precipitation in high latitudes: the need for correction. WORLD METEOROLOGICAL ORGANIZATION-PUBLICATIONS-WMO TD, 3-17.
- Goodison, B. E., Louie, P. Y., & Yang, D. (1998). WMO solid precipitation measurement intercomparison.
- Gray, D. M., & Prowse, T. D. (1993). Snow and floating ice. *Handbook of hydrology*, 7, 7-1.
- Groisman, P. Y., Koknaeva, V. V., Belokrylova, T. A., & Karl, T. R. (1991). Overcoming biases of precipitation measurement: A history of the USSR experience. *Bulletin of the American Meteorological Society*, 72(11), 1725-1733.
- Groisman, P. Y., & Legates, D. R. (1994). The accuracy of United States precipitation data. *Bulletin of the American Meteorological Society*, 75(2), 215-228.
- Harder, P., & Pomeroy, J. (2013). Estimating precipitation phase using a psychrometric energy balance method. *Hydrological Processes*, 27(13), 1901-1914.
- Harpold, A. A., Kaplan, M. L., Klos, P. Z., Link, T., McNamara, J. P., Rajagopal, S., ... & Steele, C. M. (2017). Rain or snow: hydrologic processes, observations, prediction, and research needs. *Hydrology and Earth System Sciences*, 21(1), 1-22.
- Hersbach, H., Bell, B., Berrisford, P., Hirahara, S., Horányi, A., Muñoz-Sabater, J., ... & Thépaut, J. N. (2020). The ERA5 global reanalysis. *Quarterly Journal of the Royal Meteorological Society*, 146(730), 1999-2049.
- Hydro-Québec A (1996-2022). Centrales hydro-électriques. Hydro-Québec Production. <https://www.hydroquebec.com/production/centrales.html>
- Hydro-Québec B (1996-2022). L'hydro-électricité québécoise : propre, renouvelable et faible en GES. Hydro-Québec. <https://www.hydroquebec.com/a-propos/notre-energie.html>
- Irannezhad, M., Ronkanen, A. K., & Kløve, B. (2015). Effects of climate variability and change on snowpack hydrological processes in Finland. *Cold Regions Science and Technology*, 118, 14-29.
- Jimeno-Sáez, P., Pulido-Velazquez, D., Collados-Lara, A. J., Pardo-Igúzquiza, E., Senent-Aparicio, J., & Baena-Ruiz, L. (2020). A preliminary assessment of the "Undercatching" and the precipitation pattern in an alpine basin. *Water*, 12(4), 1061.
- Kochendorfer, J., Rasmussen, R., Wolff, M., Baker, B., Hall, M. E., Meyers, T., ... & Leeper, R. (2017a). The quantification and correction of wind-induced precipitation measurement errors. *Hydrology and Earth System Sciences*, 21(4), 1973-1989.

- Kochendorfer, J., Nitu, R., Wolff, M., Mekis, E., Rasmussen, R., Baker, B., ... & Poikonen, A. (2017b). Analysis of single-shielded and unshielded measurements of mixed and solid precipitation from WMO-SPICE. *Hydrology and Earth System Sciences*, 21(7), 3525-3542.
- Kochendorfer, J., Nitu, R., Wolff, M., Mekis, E., Rasmussen, R., Baker, B., ... & Jachcik, A. (2018). Testing and development of transfer functions for weighing precipitation gauges in WMO-SPICE. *Hydrology and Earth System Sciences*, 22(2), 1437-1452.
- Larson, L. W., & Peck, E. L. (1974). Accuracy of precipitation measurements for hydrologic modeling. *Water Resources Research*, 10(4), 857-863.
- Leeper, R. D., & Kochendorfer, J. (2015). Evaporation from weighing precipitation gauges: impacts on automated gauge measurements and quality assurance methods. *Atmospheric Measurement Techniques*, 8(6), 2291-2300.
- Leroux, N. R., Thériault, J. M., & Rasmussen, R. (2021). Improvement of snow gauge collection efficiency through a knowledge of solid precipitation fall speed. *Journal of Hydrometeorology*, 22(4), 997-1006.
- Libbrecht, K. G. (2005). The physics of snow crystals. *Reports on progress in physics*, 68(4), 855.
- Marks, D., Winstral, A., Reba, M., Pomeroy, J., & Kumar, M. (2013). An evaluation of methods for determining during-storm precipitation phase and the rain/snow transition elevation at the surface in a mountain basin. *Advances in Water Resources*, 55, 98-110.
- Mekis, E., Stewart, R. E., Theriault, J. M., Kochtubajda, B., Bonsal, B. R., & Liu, Z. (2020). Near-0° C surface temperature and precipitation type patterns across Canada. *Hydrology and Earth System Sciences*, 24(4), 1741-1761.
- Nipher, F. E. (1878). *On the determination of the true rainfall, by elevated gauges*. Salem Press.
- Nitu, R., Roulet, Y. A., Wolff, M., Earle, M. E., Reverdin, A., Smith, C. D., ... & Yamashita, K. (2019). WMO solid precipitation intercomparison experiment (SPICE)(2012-2015).
- Pomeroy, J. W., & Brun, E. (2001). Physical properties of snow. *Snow ecology: An interdisciplinary examination of snow-covered ecosystems*, 45, 118.
- Quéno, L., Vionnet, V., Cabot, F., Vrécourt, D., Dombrowski-Etchevers, I., 2018. Forecasting and modelling ice layer formation on the snowpack due to freezing precipitation in the Pyrenees. *Cold Regions Science and Technology*, 146, 19–31.
- Quick, M. C., & Pipes, A. U. B. C. (1977). UBC WATERSHED MODEL/Le modèle du bassin versant UCB. *Hydrological Sciences Journal*, 22(1), 153-161.
- Rasmussen, R., Dixon, M., Hage, F., Cole, J., Wade, C., Tuttle, J., ... & Rehak, N. (2001). Weather Support to Deicing Decision Making (WSDDM): A winter weather nowcasting system. *Bulletin of the American Meteorological Society*, 82(4), 579-596.

- Rasmussen, R. M., Hallett, J., Purcell, R., Cole, J., & Tryhane, M. (2002, June). The hot plate snow gauge. In *Preprints, 11th Conf. on Cloud Physics, Ogden, UT, Amer. Meteor. Soc. P* (Vol. 1).
- Rasmussen, R., Baker, B., Kochendorfer, J., Meyers, T., Landolt, S., Fischer, A. P., ... & Gutmann, E. (2012). How well are we measuring snow: The NOAA/FAA/NCAR winter precipitation test bed. *Bulletin of the American Meteorological Society*, 93(6), 811-829.
- Ross, A., Smith, C. D., & Barr, A. (2020). An improved post-processing technique for automatic precipitation gauge time series. *Atmospheric Measurement Techniques*, 13(6), 2979-2994.
- Sevruk, B. (1989). Types of standard precipitation gauges. In *Proc. International Workshop on Precipitation Measurements* (pp. 227-236).
- Sevruk, B., Hertig, J. A., & Spiess, R. (1991). The effect of a precipitation gauge orifice rim on the wind field deformation as investigated in a wind tunnel. *Atmospheric Environment. Part A. General Topics*, 25(7), 1173-1179.
- Smith, C. D. (2009, April). The relationship between snowfall catch efficiency and wind speed for the Geonor T-200B precipitation gauge utilizing various wind shield configurations. In *Proc. 77th Western Snow Conf* (pp. 115-121).
- Smith, C. D., Yang, D., Ross, A., & Barr, A. (2019). The Environment and Climate Change Canada solid precipitation intercomparison data from Bratt's Lake and Caribou Creek, Saskatchewan. *Earth System Science Data*, 11(3), 1337-1347.
- Smith, C. D., Ross, A., Kochendorfer, J., Earle, M. E., Wolff, M., Buisán, S., ... & Laine, T. (2020). Evaluation of the WMO Solid Precipitation Intercomparison Experiment (SPICE) transfer functions for adjusting the wind bias in solid precipitation measurements. *Hydrology and Earth System Sciences*, 24(8), 4025-4043.
- Stewart, R. E., Thériault, J. M., and Henson, W. (2015). On the characteristics of and processes producing winter precipitation types near 0 C. *Bulletin of the American Meteorological Society*, 96(4), 623-639.
- Thériault, J. M., Rasmussen, R., Ikeda, K., & Landolt, S. (2012). Dependence of snow gauge collection efficiency on snowflake characteristics. *Journal of Applied Meteorology and Climatology*, 51(4), 745-762.
- Thom, A. S. (1975). Momentum, mass, and heat exchange of plant communities. *Vegetation and the Atmosphere*, 1, 57-109.
- Wolff, M. A., Isaksen, K., Petersen-Øverleir, A., Ødemark, K., Reitan, T., & Brækkan, R. (2015). Derivation of a new continuous adjustment function for correcting wind-induced loss of solid precipitation: results of a Norwegian field study. *Hydrology and Earth System Sciences*, 19(2), 951-967.
- Whitfield, P. H., Shook, K. R., & Pomeroy, J. W. (2020). Spatial patterns of temporal changes in Canadian prairie streamflow using an alternative trend assessment approach. *Journal of Hydrology*, 582, 124541.

- WMO, 2006. Representative, I. G. T. O., & Sites, M. O. A. U. Instruments and Observing Methods Report No. 81.
- Xiong, W., Tang, G., Wang, T., Ma, Z., & Wan, W. (2022). Evaluation of IMERG and ERA5 Precipitation-Phase Partitioning on the Global Scale. *Water*, 14(7), 1122.
- Yang, D. (1993). An evaluation of double fence intercomparison reference (DFIR) gauge. In *Proc. Eastern Snow Conference, 50th Meeting, Quebec City* (pp. 105-111).
- Yang, D., Goodison, B. E., Metcalfe, J. R., Golubev, V. S., Elomaa, E., Gunther, T., ... & Milkovic, J. (1995). Accuracy of Tretyakov precipitation gauge: Result of WMO intercomparison. *Hydrological Processes*, 9(8), 877-895.
- Yang, D., Goodison, B. E., Metcalfe, J. R., Golubev, V. S., Bates, R., Pangburn, T., & Hanson, C. L. (1998). Accuracy of NWS 8" standard nonrecording precipitation gauge: Results and application of WMO intercomparison. *Journal of atmospheric and oceanic technology*, 15(1), 54-68.
- Yang, D., Goodison, B. E., Metcalfe, J. R., Louie, P., Leavesley, G., Emerson, D., ... & Milkovic, J. (1999). Quantification of precipitation measurement discontinuity induced by wind shields on national gauges. *Water Resources Research*, 35(2), 491-508.
- Yang, D., Kane, D., Zhang, Z., Legates, D., & Goodison, B. (2005). Bias corrections of long-term (1973–2004) daily precipitation data over the northern regions. *Geophysical Research Letters*, 32(19).
- Yang, D. (2014). Double fence intercomparison reference (DFIR) vs. bush gauge for “true” snowfall measurement. *Journal of Hydrology*, 509, 94-100.
- Yang, Z. L., Dickinson, R. E., Robock, A., & Vinnikov, K. Y. (1997). Validation of the snow submodel of the biosphere–atmosphere transfer scheme with Russian snow cover and meteorological observational data. *Journal of climate*, 10(2), 353-373.
- Yuter, S. E., D. E. Kingsmill, L. B. Nance, and M. Löffler-Mang, 2006: Observations of precipitation size and fall speed characteristics within coexisting rain and wet snow. *J. Appl. Meteor. Climatol.*, 45, 1450–1464